INDUSTRIAL APPLICATION PAPER

Design optimization and validation for additive manufacturing: a satellite bracket application

İstemihan Gökdağ[1] · Orçun İzgü[2] · Akın Dağkolu[1] · Ahmet Alptuğ Tanrıkulu[1] · Erdem Acar[3]

Abstract

In the aerospace industry, structures are designed (or aimed) to be as light as possible to reduce emissions and carbon footprint; additionally, they are designed to improve fuel efficiency and service life while satisfying the mechanical requirements. Due to the development of additive manufacturing technology, complex structures with higher mechanical performance obtained through topology optimization (TO) can be manufactured. In this study, the overall process from part selection to qualification for a space industry-engineering application is described. First, the design space of the selected aluminum bracket is generated, and TO is performed by using stress and minimum member size constraints. The bracket is re-designed with respect to the TO output data as a reference and then the new design is validated numerically by structural analyses. The validated design is manufactured using the selective laser melting method, and heat treatment is applied to obtain more homogenized microstructure. Mechanical tests are performed on the manufactured brackets under the qualification loading conditions and post-testing examination processes are applied with metallurgical and metrological tests. According to the test results, the qualification process of the bracket is successfully completed. Consequently, the new bracket designed with TO was found to be 25% lighter than the existing design; thus, it has a huge improvement in fuel efficiency and environmental impact during the launching phase.

Keywords Topology optimization · Satellite bracket design · Additive manufacturing · Overall design process · Design for additive manufacturing · Structural optimization

1 Introduction

In recent years, the aerospace industry has been directed towards reducing the emissions and carbon footprint, additionally, increasing the fuel economy and safety of the aerostructures to be more economical and more competitive (Braga et al. 2014). Emissions of the aerospace industry have multiplied nearly two times in the last twenty years, with the industry accounting for 4.9% share of the total emissions worldwide that contribute to climate change (Lee et al. 2009). Advanced methods such as weight reduction with complex designs have significantly improved the performance of the aerospace industry products, decreased the environmental effects, as well as launching costs (a launch service to geosynchronous orbit (GEO) costs nearly $13,000/kg) (Koelle 2003; Weigel and Hastings 2004). There are two approaches to generate light-weight designs: The first approach is using advanced lower density materials, and the second one is performing structural optimization aimed at weight saving while enhancing vibration, static, and dynamic behaviors (Zhu et al. 2018). When structural optimization techniques are applied during the design phase, the mechanical performance of the structures and the efficiency of the overall vehicle can be improved with mass saving and deliver better mechanical solutions (Ide et al. 2014).

Size optimization [enabling the calculation of the optimum layout (Chen et al. 2018) and thickness of the structures (Grihon et al. 2009)] and shape optimization (to find the optimum form of structures) have been used for a long

✉ İstemihan Gökdağ
istemihan.gokdag@tai.com.tr

1   Additive Manufacturing Division, Turkish Aerospace Industries Inc., Ankara, Turkey

2   Space Systems Division, Turkish Aerospace Industries Inc., Ankara, Turkey

3   Department of Mechanical Engineering, TOBB University of Economics and Technology, Söğütözü, Ankara, Turkey

time in the aerospace industry (Edke and Chang 2006; Brujic et al. 2010; Bombardieri et al. 2021). Since Bendsøe and Kikuchi's (1988) seminal work, topology optimization (TO) method, which calculates the optimum material distribution, has started to be widely preferred during the design phase. The extensive usage of TO can be explained with some significant advantages such as not needing an initial design contrary to size and shape optimization, determining the position and number of required holes in the design space as well as deciding which section of the design should be void or solid (Zhu et al. 2016b). TO has been integrated into both academic (Liu and Tovar 2014) and commercial software with the relaxing of the numerical problems of the method (Sigmund 2007). Thus, TO method has been applied in a broad range of design processes such as pylon (Remouchamps et al. 2011), landing gear (Munk et al. 2019), fastener joints (Zhu et al. 2014), brackets (Talay et al. 2021), and fuselage (Zhu et al. 2016a).

Additive manufacturing (AM) widens manufacturing limitations with layer-by-layer material-joining process. AM is compatible with many complex structures without additional tools, molds, and complicated procedures. In addition, it does not only reduces the cost but also shortens the lead time for manufacturing (Nazir and Jeng 2020). AM applications have shown explosive growth over the last several decades due to powerful customized manufacturing capabilities. Laser Powder Bed Fusion (L-PBF) technology is one of the most common techniques for metal AM applications (Zhu et al. 2021). L-PBF has broken the shackles of the industrial application of AM with qualified components and processes from aerospace, automotive, and mechatronics to the bio-medical market (Zhu et al. 2021). To illustrate, Boeing and Norsk Titanium companies predicted about $2–3 million savings with the implementation of an FAA-approved structural titanium part to its 787 Dreamliner aircraft (Gasman 2019). Also, NASA stated that its development works on the AM subject provide up to 50% cost savings and more than 50% reduction in scheduling compared to conventional techniques (Gradl et al. 2018).

The advantages of AM technology have been coupled with TO method during the design phases. Obtaining more efficient and optimum designs have been possible with the ability to manufacture complex geometries such as lattices, internal channels, and intricate features within the part (Nazir et al. 2019). In addition, manufacturing complex TO outputs becomes possible without the need for adaptation, which is often required for the conventional manufacturing methods, with using AM methods. This design flexibility was highly appreciated in the aerospace industry as they returned with lighter and more durable designs (Stolt and Elgh 2020). Structures designed in the previous studies were exposed to thermal loading (Shi et al. 2020; Zhuang et al. 2021) and static and dynamic loadings (Savsani et al. 2017).

Space antenna bracket (Orme et al. 2017a), edge insert and star tracker bracket (Orme et al. 2017b) were designed by using TO. Moreover, qualification processes of the parts produced by AM have been completed with mechanical and metrological tests (Orme et al. 2017b; Allevi et al. 2018).

The current literature lacks a detailed description of the overall process from the part selection to the qualification of the additively manufactured satellite components. This paper aims to fill that gap along with an engineering application in the space industry. The paper is organized as follows: The overall design process of the space industry application including TO, re-design, static, vibration, dynamic, and thermo-elastic analyses is presented in Sect. 2. Manufacturing and post-process of the optimized bracket, qualification test plan, results of material and mechanical tests, assembly control, as well as metrological control are explained in Sect. 3. Finally, the conclusions drawn from this study are presented in Sect. 4.

2 Overall design process

The overall design process starts with the selection of parts suitable for AM. The design space is modeled according to the boundary conditions and equipment/adjacent part interfaces of the existing design. Then, TO problem is formulated, considering the mechanical and manufacturing requirements/constraints, and the design space and non-design space are discretized by finite elements. After the convergence criterion is satisfied, the TO result is investigated and the load paths of the bracket are determined. According to the exported TO results, the bracket geometry is re-designed in a CAD environment to be more convenient for validation analyses and AM process. Validation analyses are performed to show that the re-designed bracket meets the requirements. Then, the design process iterations are continued (progressive re-design and validation analyses) until the requirements of the satellite part are satisfied. The flowchart of the proposed overall design process is given in Fig. 1, and the validation process is described in Sect. 3 in detail.

2.1 Candidate part selection

Candidate parts to be produced by AM method have added value compared to brackets to be manufactured by the traditional subtractive method. The AM process is expensive compared to the traditional methods. The main cost comes from the powder material compared to the conventional methods; additionally, the operating machines are rarely used in the industry and their technology is relatively higher than the machines currently in use. The use of AM method has been deemed appropriate in the field of space systems where the lightness of the structures is extremely important
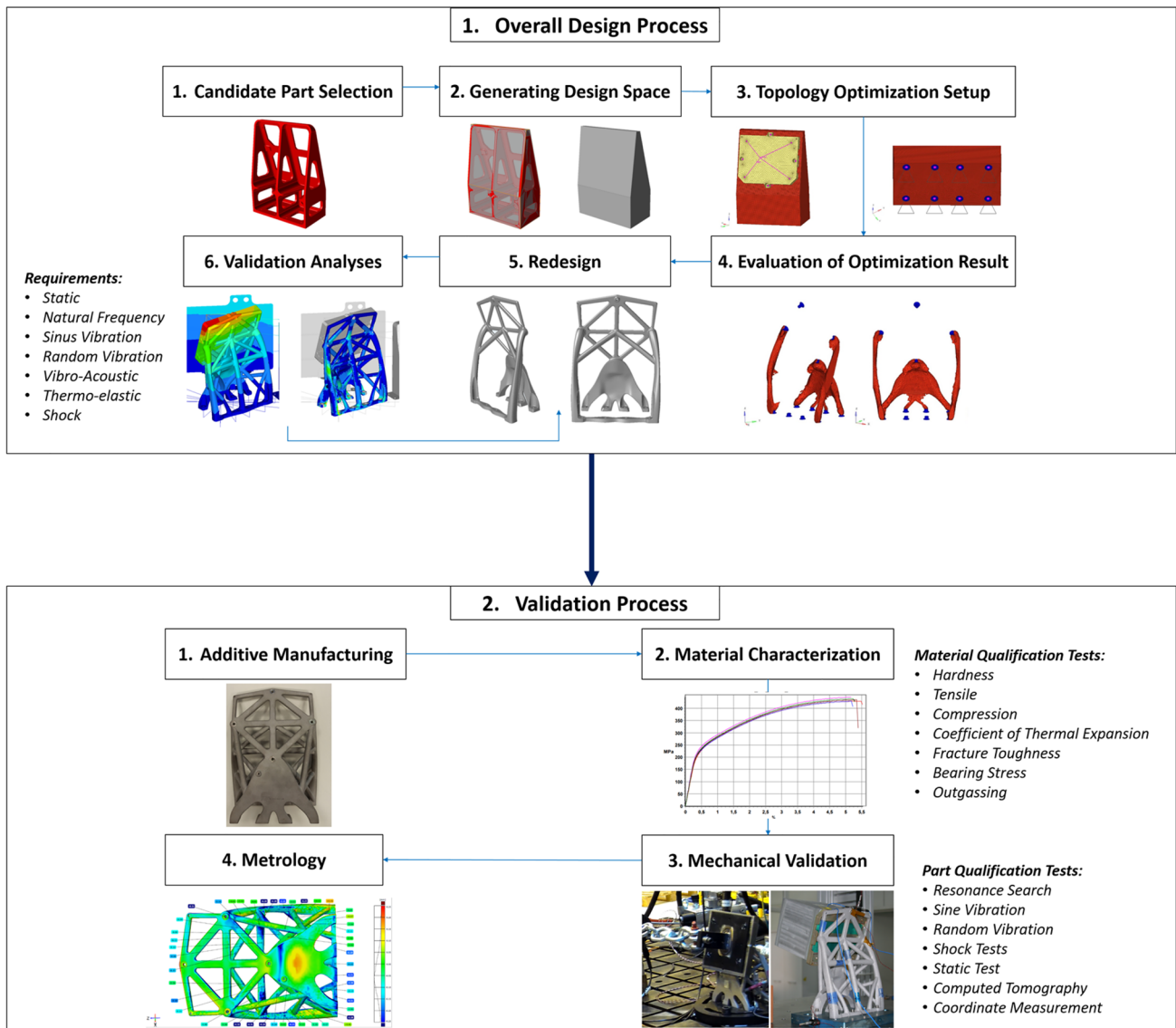
Fig. 1 Flowchart of the overall design process

and there is no need for mass production due to the rarity of spacecraft production. Added value may reduce the part's weight, increase its functionality, improve its complexity, consolidate a system of parts into one, and/or acquire higher stiffness values while simultaneously reducing its weight.

2.2 Design space definition

In TO studies, design and non-design spaces must be defined for the selected part or the system before starting with the optimization process. Design space represents the volume where the material distribution ha/s to be optimized, and the non-design space defines the areas where the boundary conditions are applied and the volume that is excluded from the optimization work. Accurate

representation of the design space has great importance in the correct definition of the optimization problem. While creating the design space, the followings steps have to be considered:

- Design space should be created in an inclusive approach covering the volume between the boundary conditions of the part. Keeping the design space as large as possible ensures that the optimization result reaches its true optimum value, while the use of a larger design space also increases the solution time because of the unnecessarily increased number of finite elements, which eventually decreases the solver performance.
- Modeled design space should not interfere with the connected or nearby parts or affect their functionality.

- While determining the design and non-design spaces, the assembly and accessibility constraints of the part intended to be optimized should be considered, and the openings for such works should be kept out of the design space. In this work, the mentioned accessibility holes are not included in the design space to save engineering time since the necessary openings are considered during the re-design phase of the optimized geometry.
- Especially in space applications, equipment should discharge the generated excess heat with conduction heat transfer. In this regard, regions that are not included in the design space are not only assessed mechanically but also evaluated for thermal loadings.
- The design space model should be as simple as possible in terms of geometry to prevent the complex mesh requirement that causes a high number of finite element usage in the finite element model (FEM).

The design space of the star tracker bracket is created in light of the aforementioned guide (see Fig. 2). The volume between the equipment and satellite body connection interfaces is preserved as inclusive as possible. The regions around the connection holes of both satellite body and equipment are defined as non-design space since the boundary conditions of the FEM setup are applied from these regions.

2.3 Topology optimization setup

In the orbital location in space without using the poles of the Earth, positioning becomes a challenge and satellites require star tracker equipment which provides a reference from the position of the stars for the location. These types of equipment consist of structural elements to attach the satellite main frames, called Star Tracker Bracket (STB). Within the application of the STB, TO problem is defined as the minimum compliance problem with the constraint functions of the force equilibrium, volume, stress, and minimum member size, respectively, as stated in Eq. 1.

$$
\begin{aligned}
&\text{Find} &&\boldsymbol{\rho} = \left[\rho_1, \rho_2, \ldots \rho_e, \ldots \rho_n\right]^T \\
&\text{Minimize} &&c(\boldsymbol{\rho}) = U^T \boldsymbol{K}(\boldsymbol{\rho}) U \\
&\text{Subject to} &&\boldsymbol{K}(\boldsymbol{\rho})U = \boldsymbol{F}(\boldsymbol{\rho}) \\
&&&\frac{V(\boldsymbol{\rho})}{V_{\text{initial}}} - V_f \leq 0 \\
&&&\text{MoS} = \frac{\sigma_{\text{yield}}}{\sigma_{\text{max}} \times SF} - 1 \geq 0
\end{aligned}
\qquad , \qquad (1)
$$

$$\text{member}_{\min} \leq 8$$
$$0 < \rho_{\min} \leq \rho \leq 1$$

where $\boldsymbol{\rho}$ is the vector of design variables including artificial density functions of each finite element, $c(\boldsymbol{\rho})$ is the compliance of the structure, U is the displacement vector, $\boldsymbol{K}(\boldsymbol{\rho})$ is the global stiffness matrix, $\boldsymbol{F}(\boldsymbol{\rho})$ is the external force vector, $V(\boldsymbol{\rho})$ is the total volume of the structure, and V_f is the targeted value of the volume fraction. In the stress constraint function, σ_{max} is the calculated maximum von-Mises stress, σ_{yield} is the material's yield stress, MoS is the margin of safety of the bracket and SF is the safety factor to keep the design in the safe zone. Thus, the stress values of the loaded structure are also taken into account while deciding whether finite elements are void or solid. Additionally, the minimum member size is integrated into the optimization problem as a constraint function to control discreteness and checkerboard effect. In addition, increasing the minimum member size also improves the manufacturability of the design. Finally, the minimum threshold value of the member size is determined considering the average mesh size.

According to the authors' design experiences, for small equipment brackets, like the one designed in this study, the natural frequency constraint is not the main driver. Rather, the static load case is the main element that drives the design. Therefore, optimization is performed using static loading conditions to reduce the computational cost of optimization.

The lift-off direction of the STB is not determined in the design process. Therefore, the bracket should be designed to carry the gravity load in all directions separately. Optimizing

Fig. 2 Creating design space for star tracker bracket
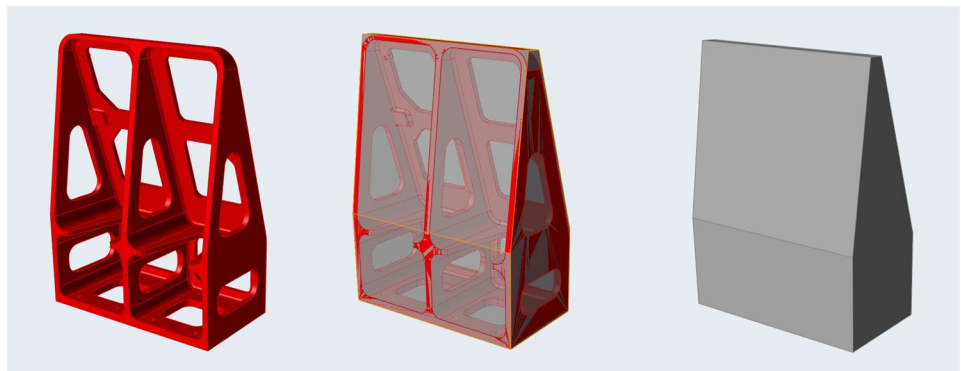
by applying forces on each axis separately would be computationally expensive. In addition, a combination of the three optimization results which are solved by applying forces separately would not be feasible in the design process. Therefore, the forces given in Table 1 are applied simultaneously on all axes during TO and the use of this approach causes increasing the MoS value of the part which is calculated in Sect. 2.5.1. Note that this practice has a shortcoming that the margin of safety obtained through this practice is larger than the one obtained when all load cases are considered simultaneously. Therefore, this practice introduces a hidden safety factor. If one chooses to consider all the cases simultaneously, then the optimization can be performed with a slight additional computational cost. Even though the sensitivity analysis will not be affected much in terms of computational cost (Bruyneel and Duysinx 2005), the optimization could take slightly more iterations.

The design space is discretized with 663,525 finite elements, and the average element size is 2.5 mm to solve the problem stated in Eq. 1. The non-design space for this problem includes the areas that should not be changed during TO and the areas where fasteners are located. The values of artificial density is the values of the elements that belong to the non-design space are taken as 1 in each iteration, so they do not participate in the TO iterations. The non-design and design spaces are shown with blue and red colors, respectively, in Fig. 3a, b.

The fastener holes shown in Fig. 3b are constrained for all degrees of freedom (DOFs) as boundary conditions. The part that connects the equipment and the bracket is modeled and incorporated in TO. Finally, the equipment is modeled as a point mass with moments of inertia values given in Table 2, and the point mass is connected to the part using 1D elements.

The results of tensile tests, performed according to ASTM E8 Standard, are given in Table 3. The details of the material testing are explained in Sect. 3.1. Test results show that the mechanical properties of the additively manufactured materials change with building directions. To keep the design on the safe side, the minimum values obtained are used in the design process for the material properties. The Poisson ratio is taken as 0.32.

The other optimization parameters are given in Table 4. The threshold value of the ρ_{min} is determined as 0.01 to avoid the singularity problems, and a plane symmetry constraint is integrated into the TO problem. The overall safety factor includes SF of AM which is 1.5 (Orme et al. 2018), and SF of yield strength which is 1.1 (ECSS Secretariat 2004). Additionally, the overall safety factor is considered as 2 during the margin of safety calculations based on TAI design practices. TO is performed using Altair Optistruct software which uses Solid Isotropic Material with Penalization (SIMP) method with the following element formulation:

$$E = \rho_i^p E_0, \tag{2}$$

where, E is the elastic modulus of the ith element calculated with penalization formulation, p is the penalty exponent, and E_0 is the elastic modulus of the solid material.

Table 1 Loading conditions

Direction	Magnitude of gravity load (g)
x	$+20$
y	$+20$
z	$+20$

Table 2 The information of the equipment modeled using CONM2 element

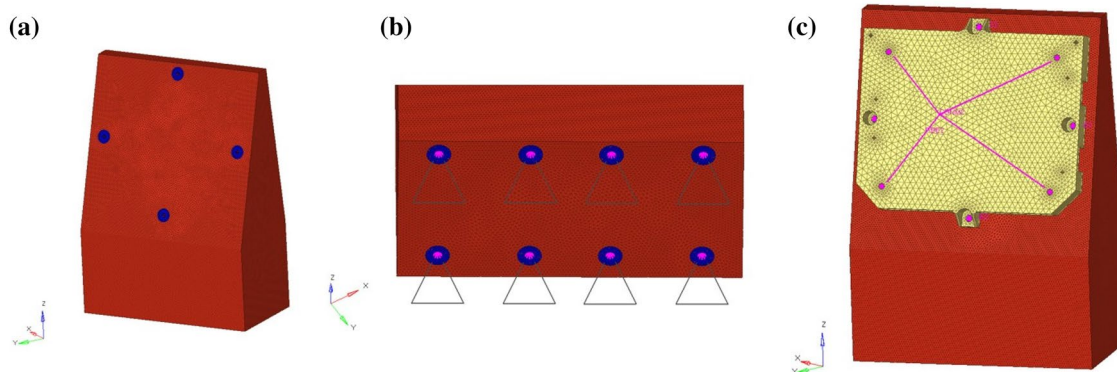| Weight (kg)	3.0		
Moments of inertia (kg·m^2)	I_{xx}	I_{yy}	I_{zz}
	0.021	0.021	0.008

(a)   **(b)**   **(c)**

Fig. 3 **a** Design and non-design spaces. **b** Boundary conditions of the structure. **c** Connection between the equipment and the bracket

Table 3 The results of tensile testing

Building direction	Elastic modulus (GPa)		Yield strength (MPa)		Tensile strength (MPa)	
	Mean	SD	Mean	SD	Mean	SD
Vertical (0°)	67.3	7.1	250.2	11.8	429.1	25.4
45°	75.9	10.4	259.2	2.3	412.8	5.2
Horizontal (90°)	77.8	4.9	265.9	5.3	408.4	6.1

Table 4 Input parameters of TO problem

Volume fraction (V_f)	5.00E−02
Safety factor (SF)	2
Minimum artificial density value (ρ_{min})	1.00E−02
Convergence tolerance	1.00E−03
Pattern grouping	Plane symmetry
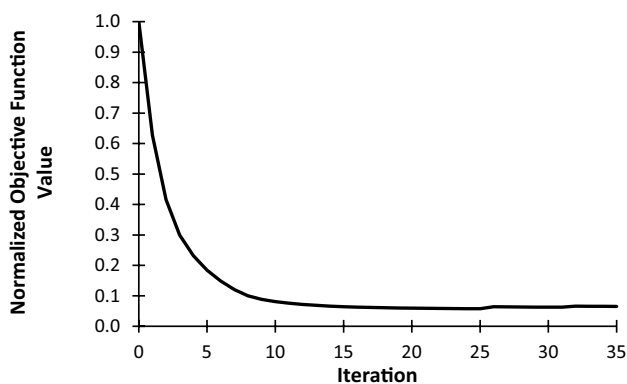
Fig. 4 Optimization history of the objective function

The TO problem is converged in 36 iterations. The variation of the normalized objective function, given in Fig. 4, shows that the normalized objective function is decreased by 93.5%. Additionally, the penalty exponent is slightly increased at intermediate iterations to achieve a more discrete solution. The penalty exponent is started at 2 initially and increased to 3 during the iterations for the minimum member size controlled TO (Altair University 2018).

2.4 Evaluation of optimization result and re-design

In the resulting optimal topology, artificial density values range between 0 and 1. This topology is visualized as density iso-surface model. The TO output consists of elements with intermediate density values, and the elements with lower density values than a predefined threshold value (based on volume constraint) are filtered and removed from the output.

The iso-surface geometry obtained from TO is only the surface of the three-dimensional space and has standard tessellation language (STL) format given by the finite elements.

This obtained geometry cannot be used in validation analyses or manufacturing steps of the part, since the geometry consists of primitive triangle faces with faulty edges, high aspect ratio elements, and unclosed surfaces. Hence, this STL geometry must be fixed with operations such as surface smoothing, element patching, etc. However, the surface-based errors such as falsely defined surface normals, gaps between surfaces/faces, and the presence of intersecting or overlapping faces make the fixing of the iso-surface model exceptionally difficult. In addition, non-design spaces and the resulting iso-surface are improperly connected. Thus, modeling the topology optimization result as a non-uniform rational B-spline (NURBS) model is more efficient in some cases.

In light of the aforementioned re-design evaluation, in the present study, after the TO, the cutoff threshold for the element filtering is set to 0.5 and the resulting iso-surface is created. As seen in Fig. 5, blue-marked non-design spaces are preserved, but the connection between the design and non-design spaces is not established. Thus, it is considered to be more efficient to re-design the geometry according to the iso-surface output. To accomplish it, firstly, the iso-surface geometry is exported in STL format, and then the body is remodeled as NURBS in a generative shape design environment. The reason for the improper connection between holes and optimized design space is that the number of holes and their positions determined in the original design are fixed and unchangeable.

With this re-design effort, the required geometry changes after the finite element analysis (FEA) are carried out more easily and quickly, such as increasing the thickness of the struts or smoothing operations at the stress concentration regions. The final CAD model of the topologically optimized and re-designed part is shown in Fig. 6. Mass saving of 25%, equivalent to 1.2 kg, is achieved comparing the original bracket designed considering conventional methods. Additionally, if the brackets have the same material, the mass saving would be nearly 21%. The weight of each bracket is calculated using the final design with relevant material.

Re-designed part geometry is rather different from the TO result since the optimization efforts are carried out considering only the static loading case of the bracket, but the bracket part also works under dynamic loadings such as vibration, shock and vibro-acoustics. TO of the part, considering all
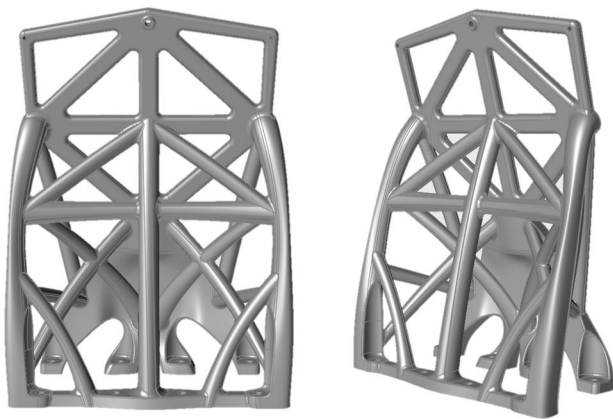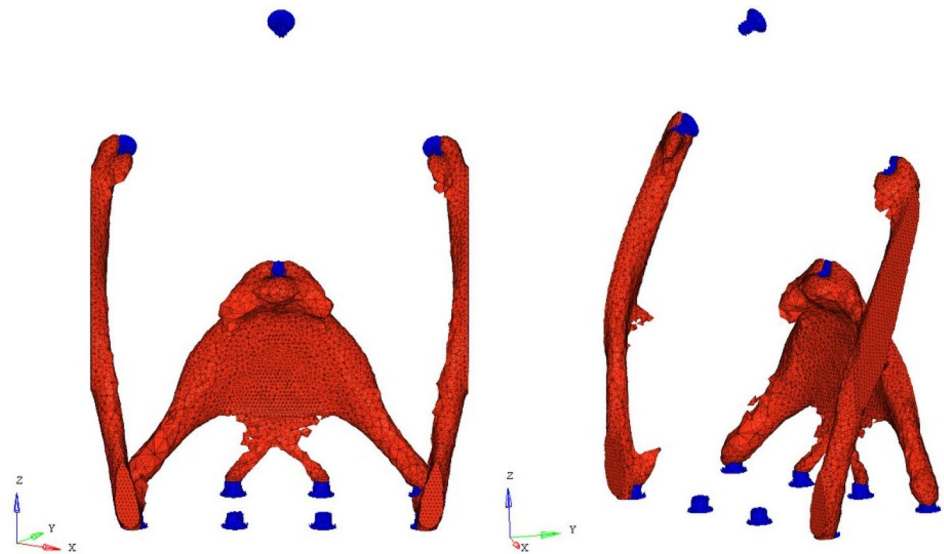
Fig. 5 Iso-surface geometry of optimized STB

Fig. 6 Re-designed NURBS model of the optimized STB

these loading conditions can be performed in two ways: (i) multi-objective TO, and (ii) single-objective TO which minimizes the volume, subject to mechanical constraints associated with these loading conditions. These suggested methods are kept out of the scope of this study and left for future works. For this reason, after each validation analysis, the part geometry is edited to its final shape to be qualified under these specified loadings. Part editing includes changing the cross-sectional areas, lengths, and angles of the strut-like bodies to acquire agile design solutions with the help of NURBS modeling. The holes at the upper left and right corners are integrated into the design to be used as alignment holes at the assembly operations, and the rods connecting them do not carry the mechanical load during the actual operation life of the part.

2.5 Validation analyses

STBs are used to carry the electro-optical equipment, which tracks the configuration of the stars to determine the position and the orientation of the satellite during its mission. To determine the structural adequacy of the equipment brackets under design loads, static, dynamic, and thermo-elastic FEA shall be performed according to launcher specifications and also environmental conditions under the specified boundary conditions by using the finite element model of the satellite system and/or subsystem. This FE application covers the first verification loop of the holistic process. If the design fails to satisfy the acceptance criteria according to the analysis results, it needs to be modified by the designer and re-analyzed afterwards. In this study, it should be noted that static, modal, random vibration, buckling, and shock analyses are performed at bracket level including the auxiliary parts such as thermal reflector, pipe support bracket, piping, etc. to include the proper mass and inertial effects, whereas thermo-elastic, sinus vibration, and vibro-acoustic analyses are conducted at satellite level to calculate more accurate results since the load types which interact with satellite structures also affect subsystems.

2.5.1 Static analyses

The main purpose of the static analyses is to ensure that the bracket structures can withstand all quasi-static acceleration loads encountered during the launch phase without excessive deformation. To obtain the effect of translational acceleration loading during lift-off, a total of three static loading cases (each perpendicular direction) are needed to be analyzed according to the ECSS-E-HB-32-26A handbook.

In this study, a certain acceleration load is applied to the brackets as a body load under proper boundary conditions in each perpendicular direction of the global coordinate system. The optimized STB is discretized by using 43,287 TET10 elements. The equipment connection and boundary conditions are modeled similar to that of the TO setup in Hypermesh software. FEM analysis setup of the optimized STB is given in Fig. 7a, and static analyses are performed by using SOL 101 Linear Static Analysis solution method of MSC Nastran software. The von-Mises stress failure criterion is used to calculate safety margins. von-Mises stress is often used to determine whether an isotropic and ductile metal will yield when subjected to a complex loading condition. This is accomplished by calculating the von-Mises stress and comparing it to the material's yield stress, which constitutes the von-Mises yield criterion. In some cases, the maximum stress location is obtained on the rigid element connection region of the brackets. These high stresses are numerical and do not correspond to physical stresses. Hence, these high stresses could be discarded in the strength evaluation of the structure. Apart from stress and deformation results, the minimum MoS value for the star tracker bracket is calculated around 6 by using the safety factor of 2. The reason for the higher MoS value is the simultaneous application of the gravity forces in TO, and the details are described in Sect. 2.3. The stress and deformation distributions corresponding to the worst-case are shown in Fig. 7.

2.5.2 Buckling analysis

Since the bracket design consists of long beams, a bracket-level linear buckling analysis is carried out to determine the minimum buckling load of the bracket system. A unit acceleration (g) load is applied in each perpendicular direction of the bracket, and linear buckling analysis is performed under the fixed boundary condition by using Simcenter 3D software. The software uses the SOL 105 Linear Buckling analysis method of NX Nastran software. During a linear buckling analysis, an eigenvalue problem is solved, and eigenvalues and eigenvectors are extracted. According to the buckling analysis results, it is concluded that the first buckling mode is extracted after 12,944 g is applied in the vertical direction. A visual of the first buckling mode is shared in Fig. 8. Under 12,944 g, it is observed that the beam extending from the front of the bracket to the rear foot is subjected to buckling. Since the calculated buckling multiplier is very high, it is decided that there is no need to perform a buckling test during the test campaign.

2.5.3 Modal analysis

Modal analyses are carried out to determine the natural frequencies and mode shapes of the bracket structure under hard-mounted boundary conditions (as safe side consideration). Modal analyses are performed in MSC Nastran software using FE mesh generated for static cases. The software uses SOL 103 eigenvalue extraction method during the solution of modal analysis. Similar to the hard-mounted boundary condition, the bracket is fixed in 6 DOFs from proper bolt locations as in static analyses.

The first three natural frequencies and related mode shapes of the bracket are calculated as a result of the modal analysis. The mode shapes are presented in Fig. 9. The
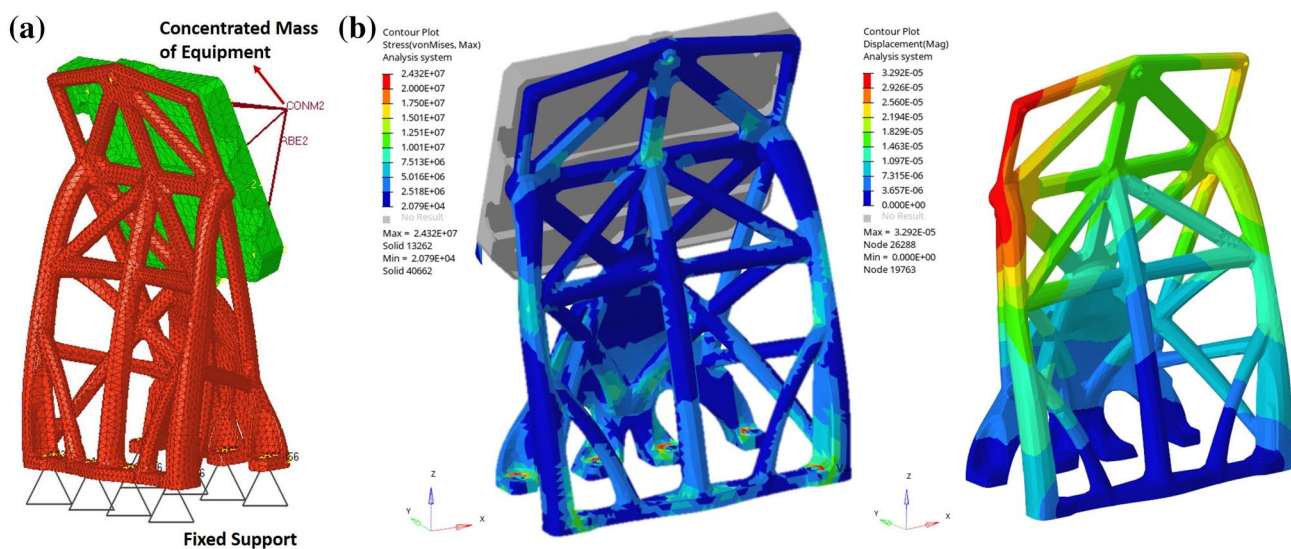

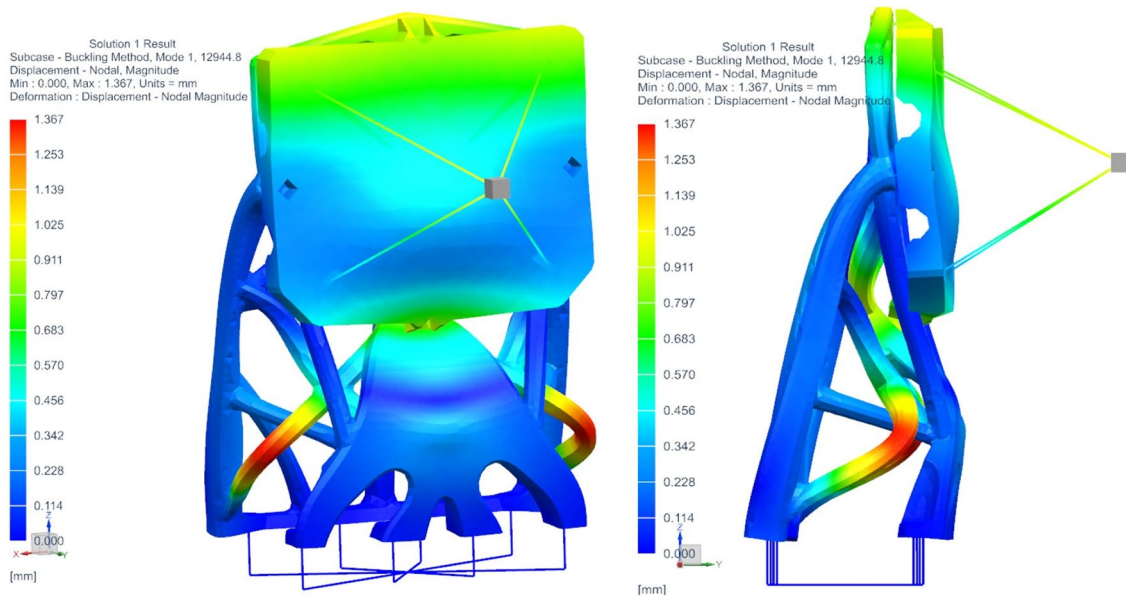**Fig. 7** **a** Static analysis setup. **b** Static analysis results of STB

Fig. 8 First buckling mode of the bracket

Fig. 9 Natural frequencies and mode shapes

1. Mode: 152.1 Hz	2. Mode: 192.7 Hz	3. Mode: 320.6 Hz

first global natural frequency is calculated as 152 Hz for the STB. No natural frequency is observed under 140 Hz, which is the minimum natural frequency design criteria for subsystems mounted on the spacecraft panels.

2.5.4 Shock analyses

Within the scope of structural qualification processes of the brackets, a series of shock analyses are performed by using both Ansys R19.0 and Simcenter 3D software in three perpendicular directions under hard-mounted boundary conditions. Simcenter 3D uses NX Nastran SOL 129 solution method during time transient shock analysis. In general, during time transient analyses, each inertial, damping, and stiffness terms of the general equation of motion are satisfied in each time step throughout the analysis time period. The mathematical model is generated with approximately 350,000 elements and 450,000 nodes.

According to ECSS-E-10-03A, satellite exposed shock level up to 0.002 s is presented in the Appendix. The shock spectrum in each direction of the three orthogonal axes is equivalent to a half sinusoidal pulse of 0.5 ms duration and 200 g (0-peak) amplitude. The damping ratio is used as 4% both in time transient and response spectrum analyses as a general approach and von-Mises failure stress criterion is used as the analysis evaluation method.

To examine the damping behavior of the system, analyses are performed for 0.1 s time period even though the load is applied for a time period of 0.5 ms (see Fig. 10). After applying the half-sine-shaped shock load, the analyzed part is left to relaxation up to 0.1 s.

The shock load is applied to the bracket system as a transient load in three perpendicular axes, and the corresponding stress levels over the analysis time and acceleration responses are calculated as output data.
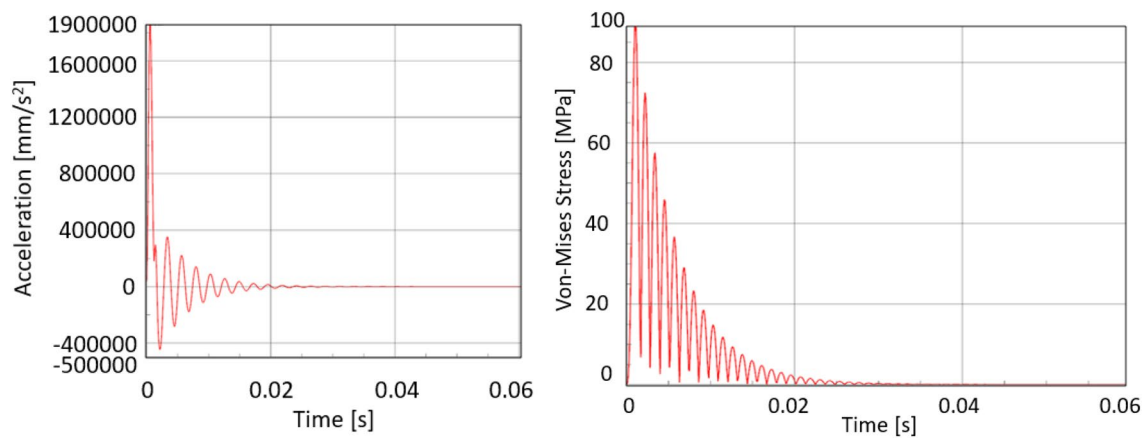
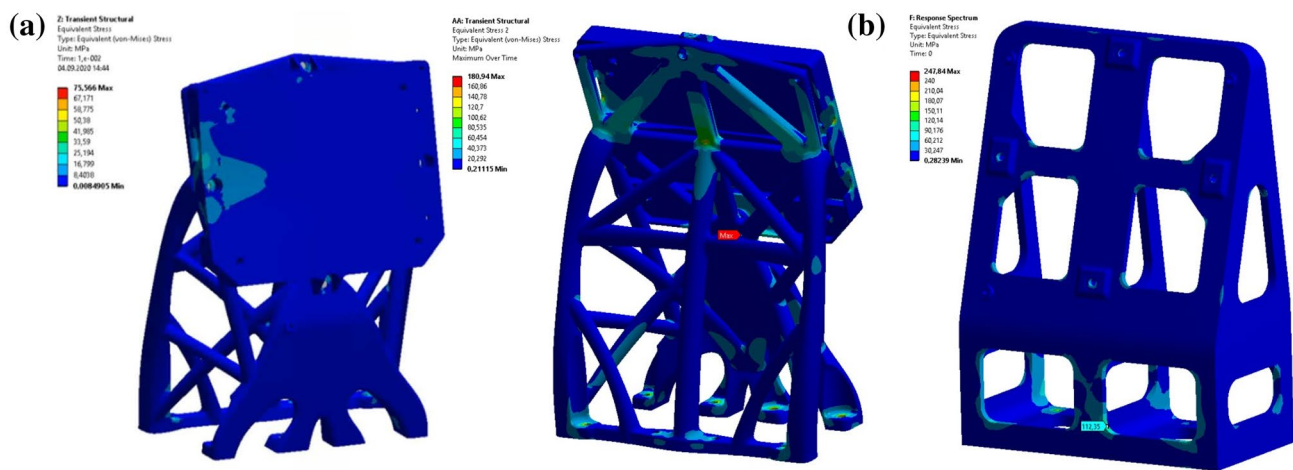**Fig. 10** Maximum acceleration and stress responses under specified damping factor

Fig. 11 von-Mises stress results **a** optimized bracket, **b** original bracket

According to the stress results of time transient shock analyses seen in Fig. 11a, the maximum von-Mises stress on the bracket is observed to remain below the yield strength of the bracket materials for all the loading scenarios. The maximum von-Mises stress is calculated as 180 MPa on the cross-section region of two struts, located in front of the bracket.

Shock analyses are also performed in three perpendicular directions on the bracket, which is designed using traditional design methodology. When the singular stresses are discarded from evaluation, the maximum von-Mises stress is calculated as 112 MPa on the corner region of a cutout in lateral direction application and it is nearly 4.2 times lower than the yield strength of the material used in the traditionally designed bracket (see Fig. 11b).

Apart from the time transient shock analyses, a series of Shock Response Spectrum (SRS) analyses of the AM bracket are also performed by using Simcenter 3D to compare the SRS responses observed during shock tests. Simcenter 3D uses NX Nastran SOL 111 Modal Frequency Response Analysis solution method during response spectrum calculations. SOL 111 generates the acceleration responses in each frequency by using the modal characteristic of the structure. Therefore, a preliminary modal analysis is performed and solutions are concentrated in the vicinity of the natural frequencies of the structure to obtain more precise results around modes. Note that the performed shock tests are shared in detail in Sect. 3.3.4. Figure 12 shows that a good correlation is obtained between the test results and analysis results, particularly in higher frequencies and maximum amplitudes.

2.5.5 Sinus vibration analyses

The main purpose of the sinusoidal vibration analyses is to investigate whether the satellite and the auxiliary
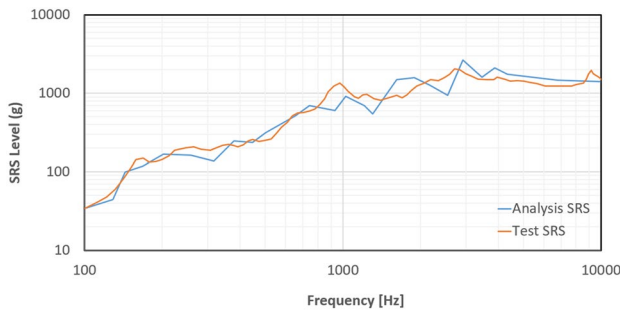
Fig. 12 SRS analysis and shock test comparison

structures can withstand sinus vibration loads encountered during the launch phase. The general idea of harmonic response analysis is to calculate the response of the structure at several frequencies and obtain a graph of acceleration quantity versus frequency. During sinus vibration analysis calculation, SOL 111 Modal Frequency Response Analysis method is used by NX Nastran software. Peak harmonic response occurs at forcing frequencies that match the natural frequencies of the structure (resonance frequencies). Therefore, before performing a harmonic analysis, the natural frequencies of the structure should be first determined through a modal solution by using SOL 103 Eigenvalue extraction method to determine accurate responses around the natural frequencies.

Calculated sinus test loads including notching are applied to the entire satellite in each perpendicular direction as body load. Acceleration responses of equipment-bracket interface location are calculated and compared with equipment qualification levels. According to the satellite-level sinusoidal vibration analysis results, when comparing both the analysis results and equipment qualification level, no exceeding value is observed from equipment qualification levels, determined from the sinus tests performed by the supplier (see Fig. 13). As a procedure, if

some exceeding values above the equipment qualification level are observed in tests or analyses, it will be necessary to perform a delta equipment qualification test by the equipment supplier or make a design change to decrease the response amplitude.

2.5.6 Random vibration analyses

Random vibration analyses are carried out under the same loading and boundary conditions as the test to have a prediction about the random-vibration tests to be performed. The mathematical model and the analysis setup are prepared by using Hypermesh software. SOL 108 Direct Frequency Response Analysis method available in NX Nastran software is used to perform random-vibration analyses. The general idea of the random-vibration analysis is to calculate the Power Spectral Density (PSD) response of the structure in the range of 20–2000 Hz from the actual accelerometer mounting location where defined in the test plan. To summarize in general terms, PSD is a conversion between the time domain and the frequency domain by using Fourier transform.

The analysis output data are compared with the optical equipment qualification level by obtaining the PSD responses. If there are any overshoots, design or accommodation changes may need to be made to keep the optical equipment on the safe side under random-vibration loading.

Random vibration test loads are applied to the bracket in each mutually perpendicular direction from the base of the bracket. According to the results of random-vibration analyses (see Fig. 14), when comparing both the analysis results and equipment qualification level, no exceeding value is observed from the equipment qualification levels, determined from the random-vibration tests performed by the supplier. Therefore, the optimized STB satisfies the equipment qualification level under the random-vibration loadings.
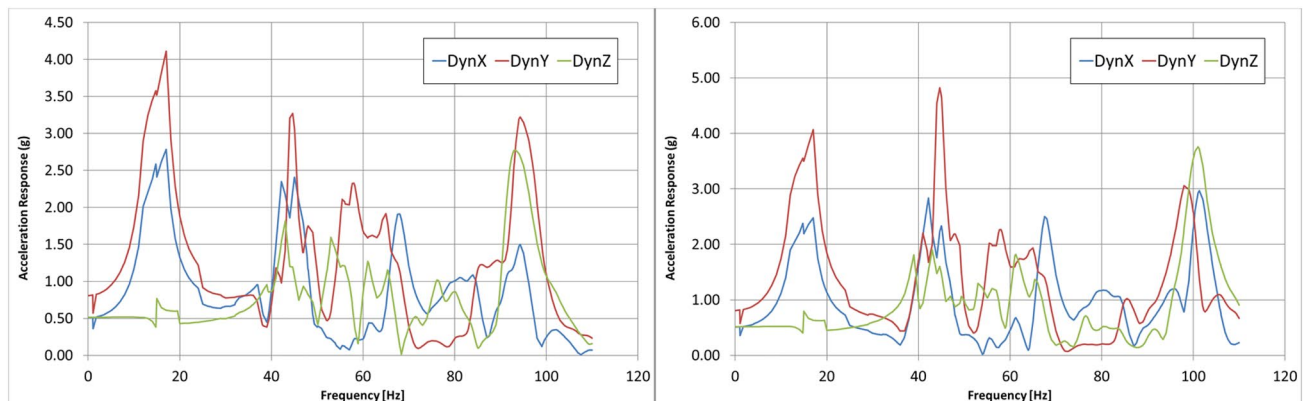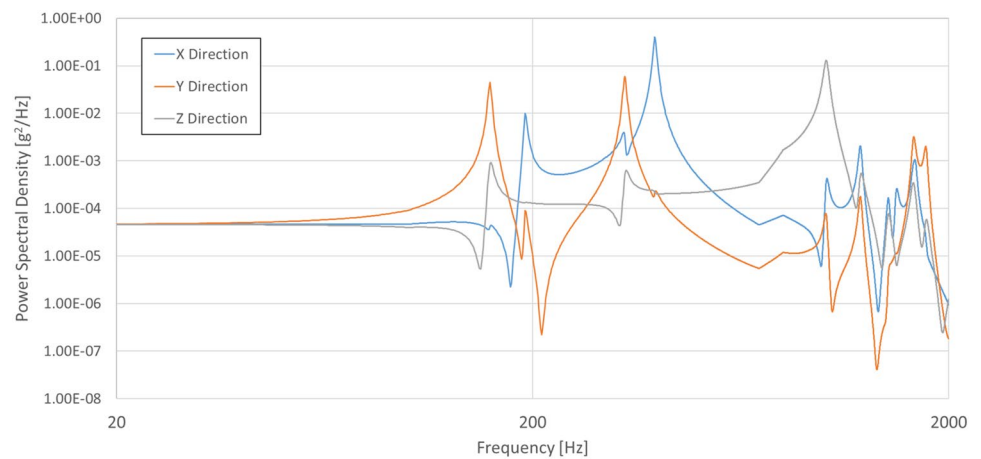

Fig. 13 Sinus vibration analyses results of STB from both in-plane and out-of-plane directions

2.5.7 Thermo-elastic analyses

Satisfactory performances of the brackets require accurate prediction of thermal deformations to verify pointing and alignment accuracy requirements for sensors. Therefore, it is important to calculate the angular positioning deviations for high-precision equipment like star trackers. These values must not exceed the deviation limits specified for precise mounting. In this part of the structural analysis studies, the thermal displacements are calculated under on-orbit thermal conditions for the STB.

In thermo-elastic analyses, under Equinox, Winter Solstice, and Summer Solstice thermal scenarios, the relative displacements between star tracker bracket and antennas are calculated. As a procedure, the thermal input is supplied from the thermal control subsystem by performing time transient analyses under in-orbit boundary conditions and implemented on the whole satellite by the structural analysis team.

According to the pointing analyses results, no incompatibility is found in means of thermal deformation and rotation tolerances of the optic equipment. The rotation tolerances should be within the mission requirement determined by the program management division of the project. According to the results of thermo-elastic analyses shown in Fig. 15a, it can be stated that the rotation results of the STB (high-precision equipment) are found to be within the tolerances of the project management.

Apart from satellite-level thermo-elastic analyses, bracket-level analyses are also conducted and maximum displacement and stress values are checked under the worst-case scenarios. The analysis results are shown in Fig. 15b. During thermal stress analyses, SOL 101 Linear Steady-State Heat Transfer method is employed by using the coefficient of thermal expansion of the material. Using the computed thermal strains, thermal stresses are calculated for bracket structure in steady-state conditions.
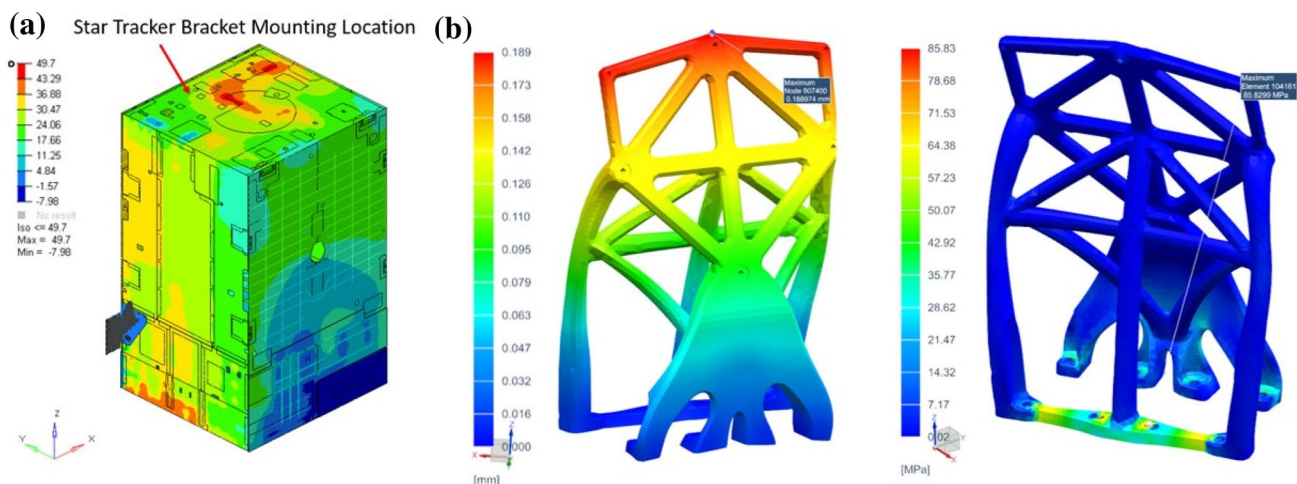

Fig. 15 **a** Thermo-elastic analysis results in terms of satellite-level thermal distribution. **b** Bracket-level thermo-elastic analysis results

According to the analysis results, maximum displacement and von-Mises stress values are calculated as 0.18 mm and 85 MPa, respectively. Maximum displacement value is evaluated within acceptable tolerances, and maximum stress value is considerably lower than the acceptable value of the material.

2.5.8 Vibro-acoustic analysis

During the lift-off, a spacecraft assembly and auxiliary equipment are subjected to high vibro-acoustic loads, generated through combustion into launcher engines. These loads range from 0 to 10,000 Hz, and they can cause damage to satellite structures due to their high amplitudes. Therefore, acoustic tests are necessary to validate the general behavior of the satellite structure and its dynamic compatibility with its subsystems and the equipment under an acoustic environment. Before the test campaign, a prediction of acoustic tests needs to be carried out by taking high-performance computer aid. A vibro-acoustic analysis is performed by using Simcenter 3D software to simulate the subjected noise effect on satellite structures during the lift-off. Simcenter 3D software uses NX Nastran SOL 111 Modal Frequency Response Analysis method with preliminary modal analysis.

During a vibro-acoustic analysis of a satellite project, in general, PSD output is obtained from the accelerometers located on the equipment-bracket interface, and compared with the qualification level of equipment to predict damage to the equipment during the acoustic test. Note that it is sufficient to calculate the vibro-acoustic analysis by using FEM up to 500 Hz because of the following three reasons: (1) acoustic noise input levels at high frequencies are 10 dB and more below the peak input in the 250 Hz octave band,

(2) response at high frequencies exhibits low deformation and consequently low stresses, and (3) their contribution to the total root-mean-square acceleration (gRMS) response is relatively low (Ruess et al. 2016).

Satellite mesh and air-represented acoustical cavity mesh are shown in Fig. 16a. The acoustic plane waves surround the entire satellite system as a spherical shape to generate uniform sound pressure levels on the entire spacecraft, with proper boundary conditions. To get accurate results, a mesh convergence study is also performed on the satellite structure during the modeling phase.

Plane-wave generators that represent the monopoles are modeled to reflect the actual acoustic test boundary condition. As a boundary condition, one-noded fixed support is defined on the master node of the satellite located on the geometric center of the clamp bands (see Fig. 16c).

According to Ariane 6, Falcon 9, and Proton M launcher specifications, acoustic loads that a satellite is exposed to during the lift-off are presented in Fig. 17. When the acoustic loads of the three candidate launchers are examined, the highest amplitudes at all frequencies belong to the Proton M launcher. Therefore, loads of the Proton M launcher are used as the input to stay on the safe side in the vibro-acoustic calculations. Both in-plane and out-of-plane direction responses of the equipment–bracket interface region are examined up to 500 Hz under vibro-acoustic load.

As an output of the analysis, PSD response graphs generated from the exact accelerometer location can be seen in Fig. 18. According to the satellite-level vibro-acoustic analysis results, when comparing the analysis results and equipment qualification level, it is concluded that no exceeding value is observed from equipment qualification level, determined from the random-vibration test performed by the equipment supplier. The qualification test input is supplied
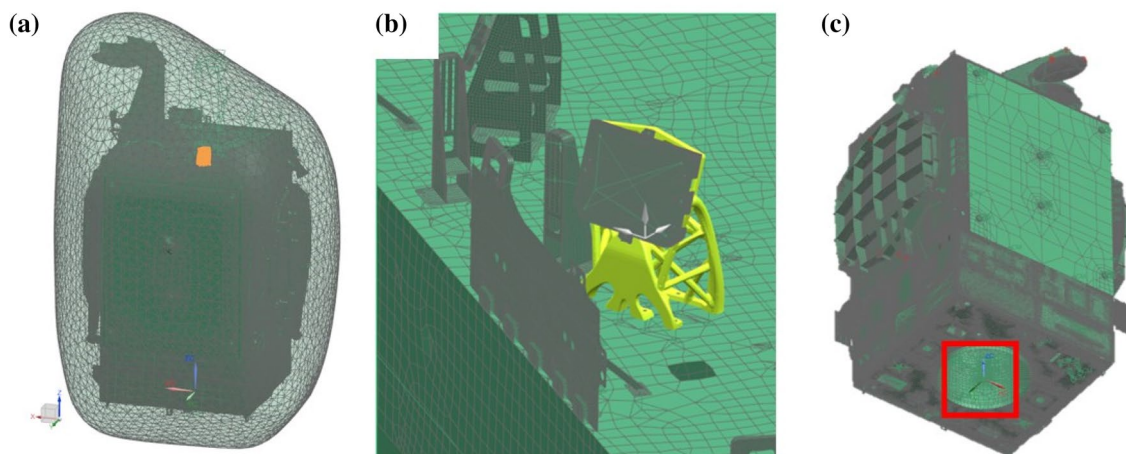

Fig. 16 **a** Communication satellite structure mesh, air-represented cavity mesh. **b** Bracket location detail. **c** Location of fixed support boundary condition

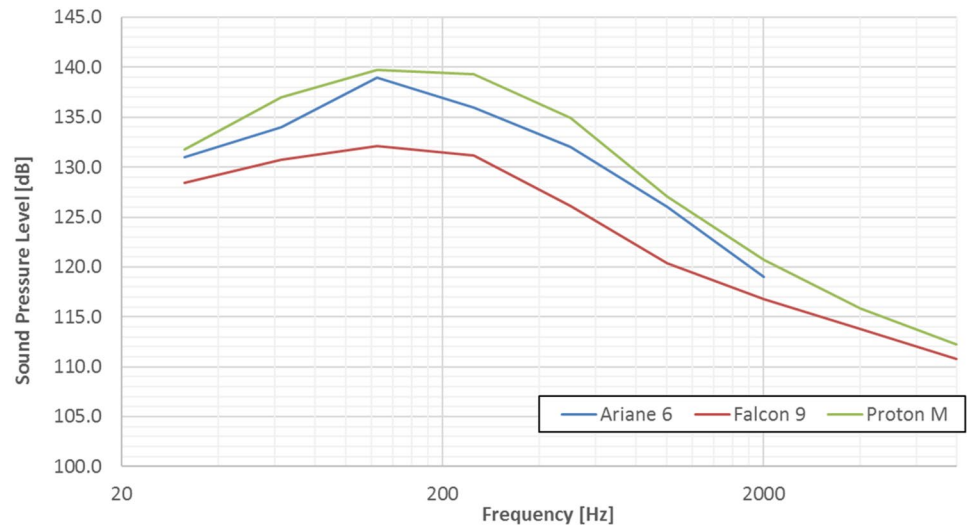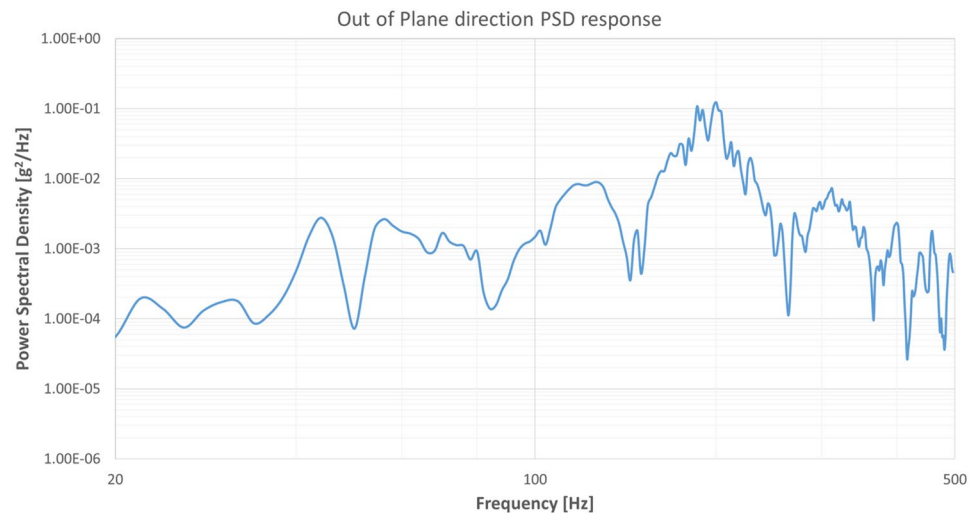**Fig. 17** Candidate launcher's acoustic load spectrum

Fig. 18 Power spectral density response of out-of-plane direction

by the equipment supplier which limits the publication of the data for the present study regarding confidentiality. The PSD response obtained from the vibro-acoustic analysis is shown in Fig. 18, below. Since the most critical response is obtained in the out-of-plane direction, only the out-of-plane response is shared.

3 Experimental validation and qualification

3.1 Material testing

While the process characteristics and the chemical composition define the material properties, numerical studies, validation analyses, mechanical tests, and microstructural characterization give detailed information about the AM-built materials. Compared to the conventional manufacturing processes, shorter design cycles, very rapid solidification,

cooling rates, and flexible products are obtained by AM. According to the complexity of the material design and production rates, it is often difficult to produce cost-effective parts by AM; however, with the improvements of the AM technology, it has become possible to produce end-use parts, especially in the aerospace industry (the fastest growing sector followed by automotive industry). Hence, the AM-built materials have complex and unstable microstructures, and these microstructures should be fully understood by material scientists to develop a comprehensive material allowable database for design engineers. Therefore, a wide range of material tests are conducted in the present study, specific to L-PBF AlSi10Mg (see Table 5).

Material tests listed in Table 5 are conducted according to the service condition of the selected component. It is known that AM materials have anisotropy inherently due to the technology employed for the process. Thus, all tests are conducted for three different orientation angles; 0°, 45°,

Table 5 Material tests and standards

Qualification	Test	Standard or reference
Material characterization	Hardness	ISO 6506-1/2
	Tensile	ASTM E8
	Compression	ASTM E9
	Coefficient of thermal expansion	ASTM E228-17
	Fracture toughness	ASTM E399/ASTM B646-19
	Bearing stress	ASTM E238-17a
	Outgassing	ECSS-Q-70-02
	Fatigue	ASTM E466

and 90°. The lowest mechanical properties are observed in specimens that are manufactured in the vertical direction with respect to the building platform. Hence, these mechanical properties are used in the design phase to stay in the safe zone. Mechanical tests are executed to obtain the material properties, while thermal and outgassing tests are conducted to obtain the required pass-fail criteria of the service condition in space. However, the component is not exposed to cyclic loading during the mission, and plastic properties of the material are evaluated to make a full understatement of the fracture behavior of the AM microstructure. Consequently, fracture toughness, bearing stress, and fatigue tests are conducted in addition to the tension/compression tests following related standards (see Table 5). In addition to material tests, metallurgical analyses including fractography, EDS analysis, electron, and optical microscopy imaging are performed to investigate the microstructure of the material in detail.

3.2 Additive manufacturing and post-processing

The original STBs are manufactured with machining operations with Al7000 series material. In this study, optimized and re-designed STBs are manufactured with AM methods with the most commonly used AM alloy, AlSi10Mg. The final design of the STB consists of intricate and bionic-formed strut bodies which are impossible to form with machining operations. Other than AM, the only conventional manufacturing process that could be employed is the casting method. Selecting the casting method to manufacture a geometry with this level of complexity requires the usage of multiple casting molds and cores which eventually increase the lead time and cost considering the required manufacturing quantity, which is considerably low in space applications. The unit cost of AM and its post-processes are relatively high with respect to conventional methods, but the ability to manufacture complex and lighter designs compensates for this manufacturing cost. For the AM of the brackets, L-PBF method is employed since this technology has higher industrial accessibility and gives better surface roughness than other metal AM methods such as
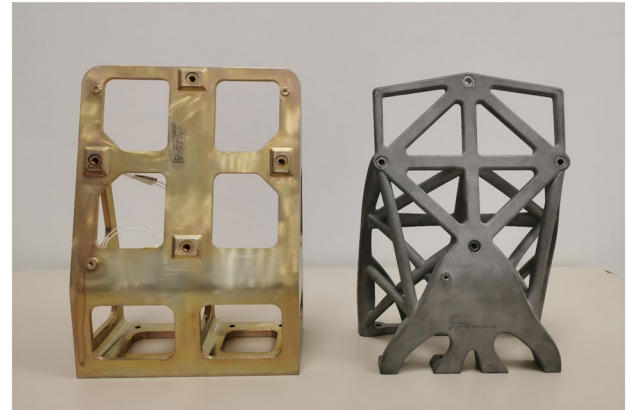

Fig. 19 Existing design (left) and optimized design (right) of STB

EBM or binder jetting. Re-designed STBs given in Fig. 19 are manufactured by using selective laser melting (SLM) Solutions-SLM 500® machine. Eight brackets are manufactured through AM by using the same powder batch. SR2 heat treatment condition in accordance with ASTM F3318 standard is applied to improve the mechanical properties using Argon-backfilled HT furnace. The heat-treated brackets are machined to ensure the desired tolerance values of the assembly surfaces. The tolerance requirement includes the flatness, the tribological surface quality of the assembly surface, and the relative positions of the mounting holes.

3.3 Mechanical validation

Two types of tests (material-level tests and bracket-level tests) are conducted during the qualification of the bracket structures. Material-level tests are performed to qualify the material itself since there is no qualification history for AlSi10Mg material inside the company. Bracket-level tests are conducted to qualify the bracket structures as a final product. Performed tests and used standards for the material qualification are listed below. Apart from the mechanical tests, CT and coordinate measurement tests are also conducted to get detailed information about the inner characteristics of the structure. Conducted test campaign for material

**Table 6** Material and part level test campaign

Qualification	Test	Standard or reference
Part qualification	Resonance search	TAI-T025
	Sine vibration	TAI-T025
	Random vibration	TAI-T025
	Shock tests	TAI-M0250
	Static test	TAI-T023
	Computed tomography	NA
	Coordinate measurement	NA

characterization and part level qualification and corresponding company internal standards are given in Table 6 in detail.

In addition to material level tests in Sect. 3.1, bracket-level resonance search tests before and after sinus vibration, random-vibration and shock tests, static tests, and thermal cycle tests are conducted during the qualification process of the additive manufactured STB.

3.3.1 Dynamic tests

Dynamic tests aim to validate the dynamic responses of STBs and their mechanical behavior under dynamic qualification loads. The objective of the dynamic test is to demonstrate the dynamic characteristics of brackets during the application of sinusoidal, random vibration, and shock loads under proper boundary conditions. The dynamic test setup of the optimized star tracker can be seen in Fig. 20. During dynamic tests, representative dummies are designed and mounted on the brackets with the original fasteners and washers not to damage the real optical equipment. Bracket-test fixture connections are also supplied with original titanium bolts to reach the most realistic force distribution and get information about fastener performance. To check whether there is any structural integrity disruption on the bracket structures, low-level resonance search tests are
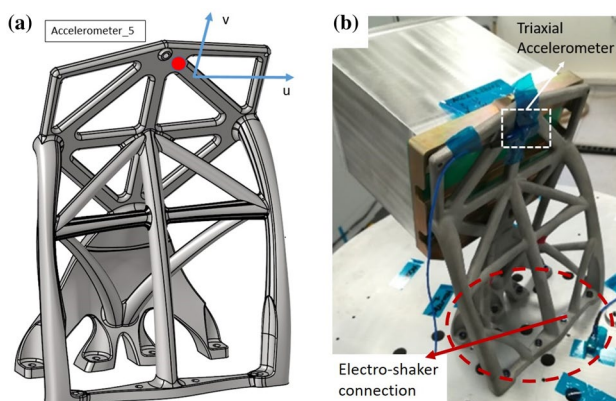
performed before and after qualification level vibration tests and compared to each other to verify the related requirement statement. The instrument mounting location and directions are presented in Fig. 20.

The qualification test input is supplied by the equipment developer, and it is limited in terms of sharing according to the project confidentiality. Before each sine and random vibration test, resonance search, and sine sweep test are conducted with the inputs and parameters given in Table 7.

Before the test campaign, the success criteria of dynamic tests are determined as follows: (1) The overall structural integrity of the brackets should be preserved and no visible crack should be detected. (2) The frequency difference of the main modes of the structure in the resonance search tests performed before and after the qualification level tests should be less than 5%. (3) The magnitude difference of the main modes of the structure in the resonance search tests performed before and after the qualification level tests should be less than 20%. (4) According to coordinate measurements performed before and after the tests, relative deflection values over the flat surfaces should be within the tolerances.

Before and after each qualification test, a low-level sine sweep test is conducted to see if there is any structural integrity deterioration occurred on the structures during qualification tests. The comparison of before and after low-level tests is presented in Figs. 21 and 22. Even if before-after test comparisons of Y-axis test are given in the relevant figures, these comparisons are repeated for each direction.

According to the dynamic testing results, all of the following success criteria are satisfied.

1. No visible crack is detected after the test campaign is completed.
2. Frequency differences of the main modes remained below 5%.
3. Amplitude differences of the main modes remained below 20%.
4. According to the coordinate measurements, the relative deflection values over the flat surfaces (the most critical parameter, since the brackets carry the optic sensor) values are within the specified tolerances.

3.3.2 Static tests

A static test campaign is planned to be performed to verify the strength of the equipment brackets under quasi-static qualification loads and screening for potential failures.

Fig. 20 a Accelerometer mounting location. **b** Vibration test setup

Table 7 Sine sweep input

Frequency band [Hz]	Acceleration [g]	Sweep rate [oct/min]
0–1000	0.5	2

Fig. 21 Low-level resonance test graphs, comparing the condition of the bracket before and after sinus vibration testing
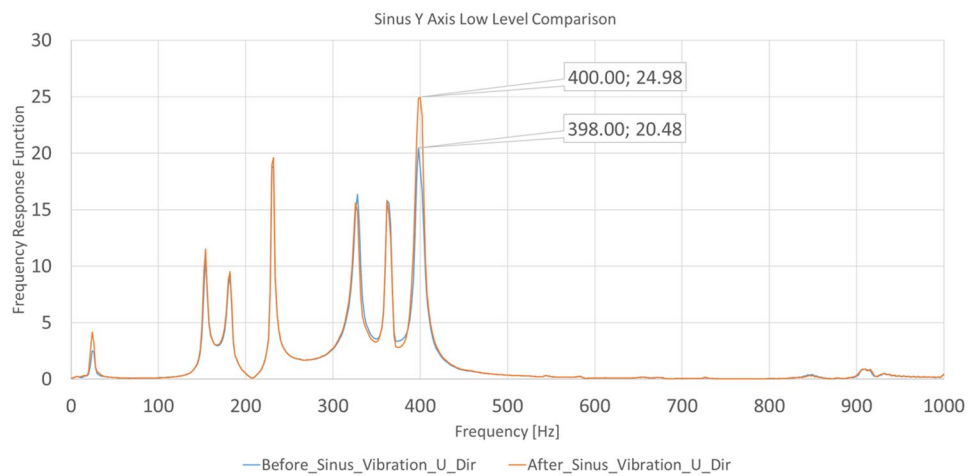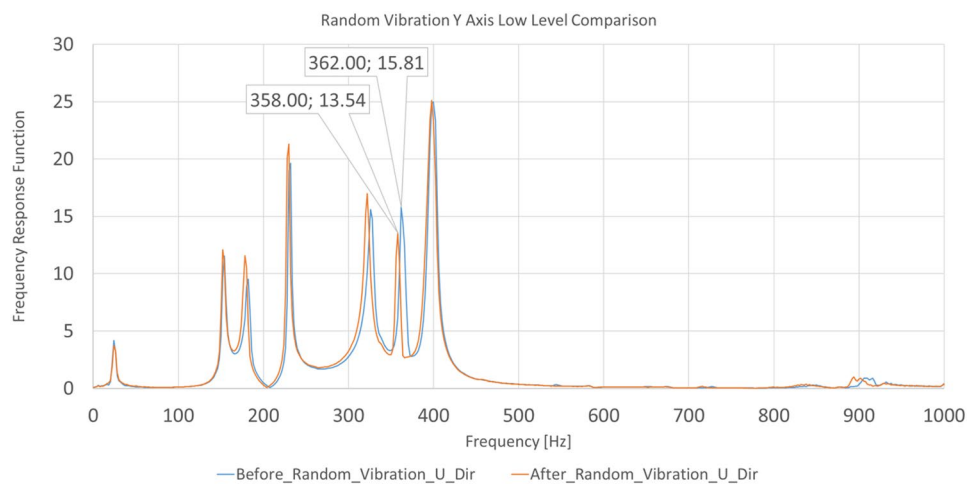
Sinus Y Axis Low Level Comparison

400.00; 24.98
398.00; 20.48

— Before_Sinus_Vibration_U_Dir   — After_Sinus_Vibration_U_Dir

Fig. 22 Low-level resonance test graphs, comparing the condition of the bracket before and after random-vibration testing

Random Vibration Y Axis Low Level Comparison

362.00; 15.81
358.00; 13.54

— Before_Random_Vibration_U_Dir   — After_Random_Vibration_U_Dir

The qualification test load of the equipment bracket is obtained according to the ECSS-E-HB-32-03C handbook. Part qualification is evaluated after the test with respect to the following two success criteria: (1) No cracks, permanent deformation or any kind of failure should occur after qualification load sequences at the end of the test. (2) Load–strain curves measured from strain gages should demonstrate linear character during nine times repeated tests.

The static test setup of the optimized STB is given in Fig. 23a, b. According to the material test results obtained from tensile tests, the maximum strain value of the material that showed linear characteristics is determined around 3000 μ strains. According to the evaluations carried out with this information, no plastic strain is measured that could cause permanent deformation from any strain gage up to the limit load which corresponds to the maximum test load.

An example from a strain gage response is shown in Fig. 23c. It can be seen that the maximum application load (which corresponds to the design limit load of the equipment bracket) is far from the plastic zone of the material.

On the other hand, since the residual strain values measured by sensors are very close to zero when the load on the bracket is released, it is concluded that there is no permanent deformation.

3.3.3 Thermal cyclic tests

According to the satellite-level thermal analyses with on-orbit boundary conditions, the equipment brackets are subjected to the thermal loading within the range of – 50 °C and + 60 °C, which corresponds to the worst case of on-orbit temperatures. To check the structural integrity preservation of brackets under thermal loading, a cyclic thermal test is performed. In the tests, the temperature of each equipment bracket is measured by using PT100 sensors. The test is planned as ten cycles, and brackets are held at each thermal peak for 5 min (see Fig. 24). Before the test campaign, the success criteria of thermal tests are determined as follows: (1) No visible crack should be detected. (2) According to coordinate measurements performed before and after the
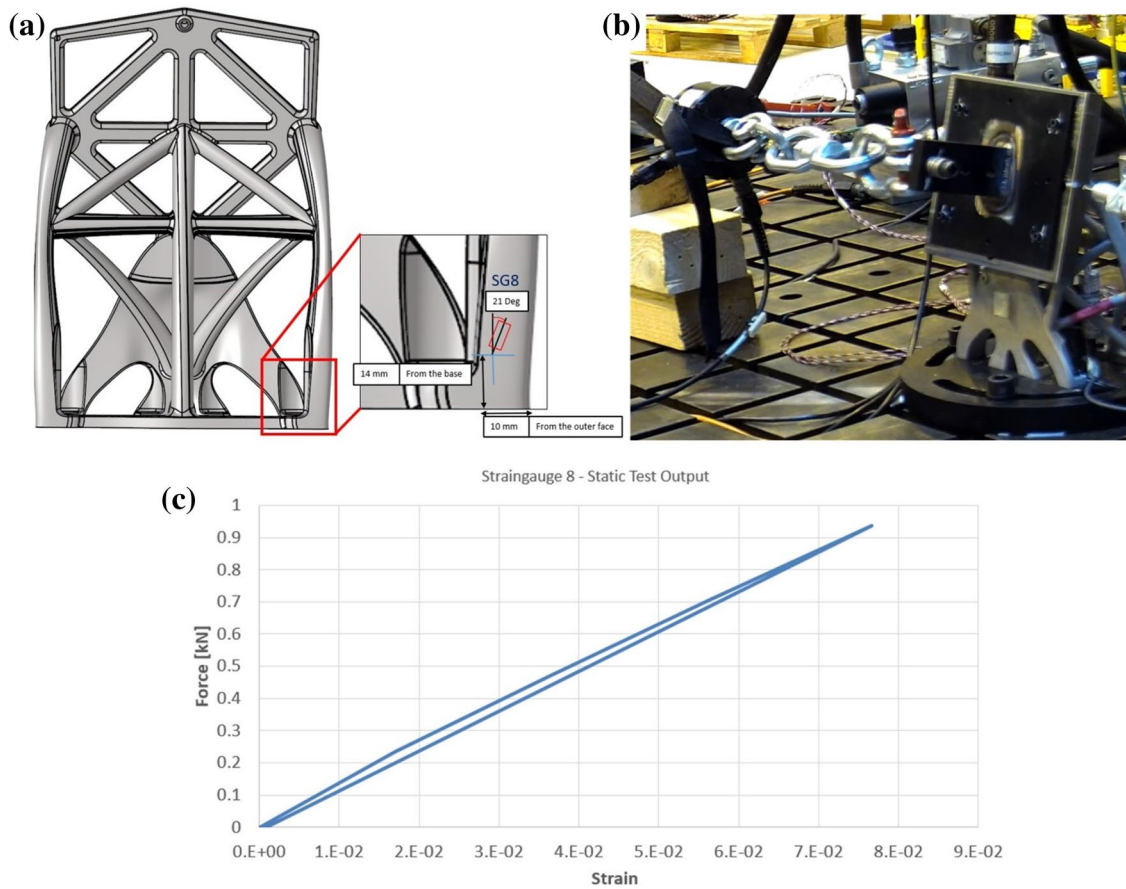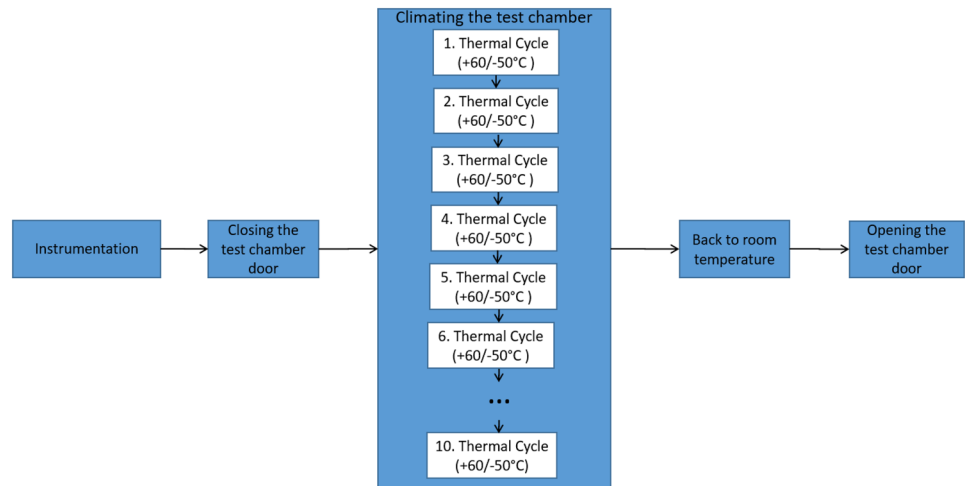
Straingauge 8 - Static Test Output

Fig. 23 **a** Strain gage mounting locations. **b** Static test setup. **c** Force vs strain graph of strain gage #8 in the static test

Fig. 24 Thermal cyclic test sequence

thermal tests, relative deflection values over the flat surfaces should be within the specified tolerances.

The test sequence and corresponding thermal test results can be seen in Figs. 24 and 25b, respectively. During the thermal cycle test, temperature values are monitored by a thermistor sensor placed on the bracket. The thermistor connection location is as in Fig. 25a. According to test results, test success criteria are successfully achieved with coordinate measurement result comparison of before and after
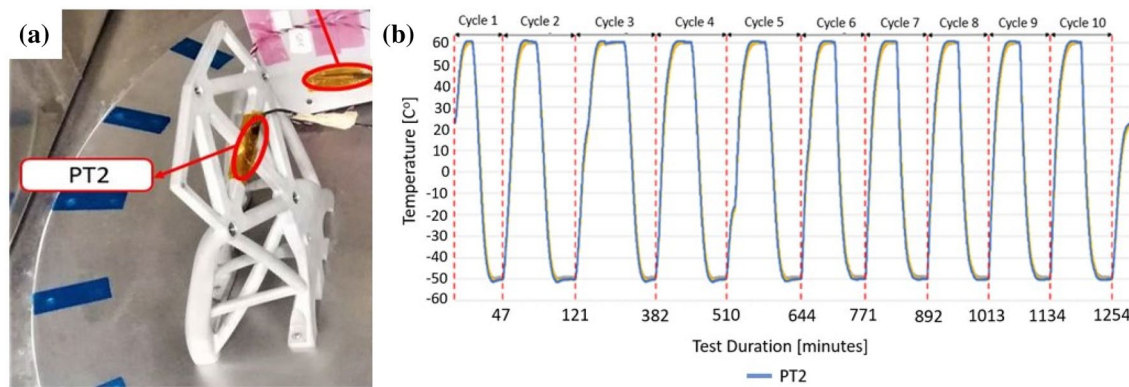
Fig. 25 **a** Thermistor sensor location. **b** Temperature variation data acquired from the PT2 sensor during the thermal cyclic test

thermal test campaign. The measured values are within the specified tolerances.

3.3.4 Shock test

The main purpose of the shock test is to investigate whether the bracket structure can withstand the shock loads encountered during clamp band separation and pyro bolt detonation of solar array panels and reflector antennas. The envelope of the shock loads that will occur during the satellite's mission is calculated, and the maximum acceleration loads over frequencies are applied during the tests as SRS loads. As a procedure, a set of trial tests are carried out on a dynamic representative dummy equipment bracket until the specified acceleration levels are achieved. After achieving the qualification level on the dummy equipment bracket, the principal equipment bracket is connected to the test setup, and the test is performed in three runs in each direction by using the qualification load. A pyro-shock test device, which throws a projectile-like material underside of the test adapter, is used during the tests. After each test, SRS levels are generated by a KiStudio Lab software and compared with the specified equipment qualification level. If the SRS level measured after the test remains below the specified level, the test is repeated by increasing the pressure load of the device. Before the test campaign, the success criteria of shock tests are determined as follows: (1) The overall structural integrity of the brackets should be preserved and no visible crack should be detected. (2) The frequency difference of the main modes of the structure in the modal hammer tests performed before and after qualification level tests should be less than 5%. To measure that the second success criterion is met, before and after the shock tests, a series of modal hammer tests under free-free boundary conditions are performed and compared with each other to determine the structural integrity preservation of the brackets.

Six accelerometers are used, which measure three mutually perpendicular direction responses both the equipment-bracket connection region and bracket-satellite interface region (see Appendix). Before and after each shock test, a series of modal hammer tests are conducted under free-free boundary conditions by hitting several points of the bracket. Then, a before-after comparison is conducted in terms of natural frequency responses of main modes up to 2000 Hz to check the structural integrity preservation of the bracket. A before-after shock test comparison example of modal hammer test output can be seen in Fig. 26.

It is concluded that there is no visible crack observed on the test specimens, and according to the comparison of before/after modal hammer test output, the natural frequencies are within the tolerances of 5% which are specified in the success criteria definition before the test campaign. The reason for the difference in amplitudes is that the test performer does not strike at the same speed each hit. Depending on the hit speed, the amplitude may change due to the damping factor, and therefore, no success criteria have been determined in terms of amplitude difference before the shock tests.

3.3.5 Metrology

After manufacturing and post-processing efforts, critical part dimensions are measured with the coordinate measurement method. Coordinate measurements are applied to the fastener holes and the contact surfaces of the part, and it is found that manufactured part feature dimensions comply with the required geometrical tolerances. In addition to that, before and after the static, dynamic, and thermal tests, coordinate measurement and 3D geometrical scans are applied to evaluate if there are any geometrical deviations between the tests. Coordinate measurements are applied to the exact locations as former measurements and the 3D scan is applied to the entire geometry. According to the comparison of the
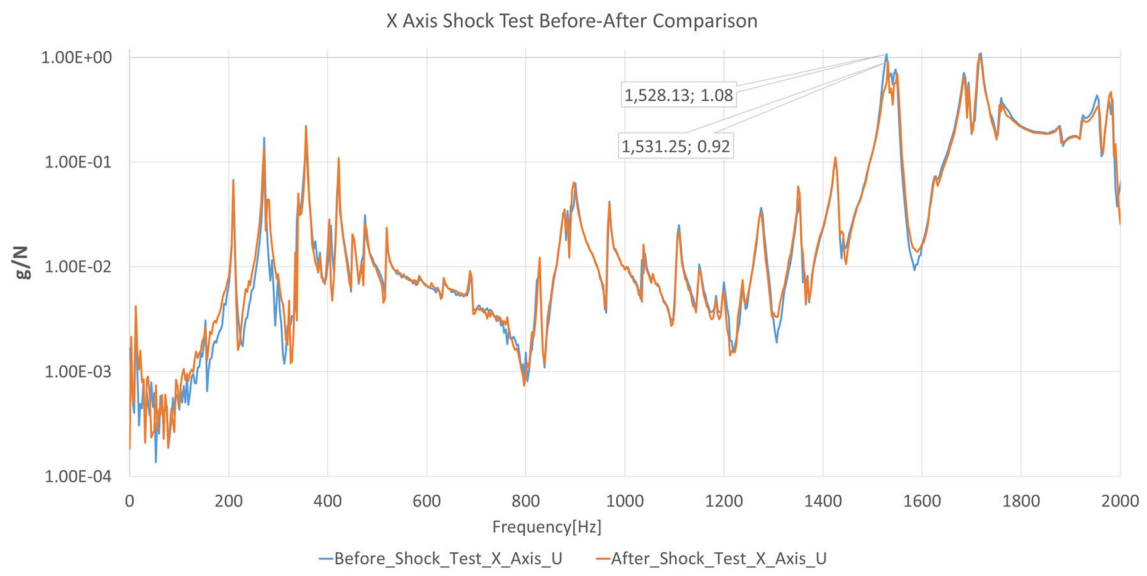
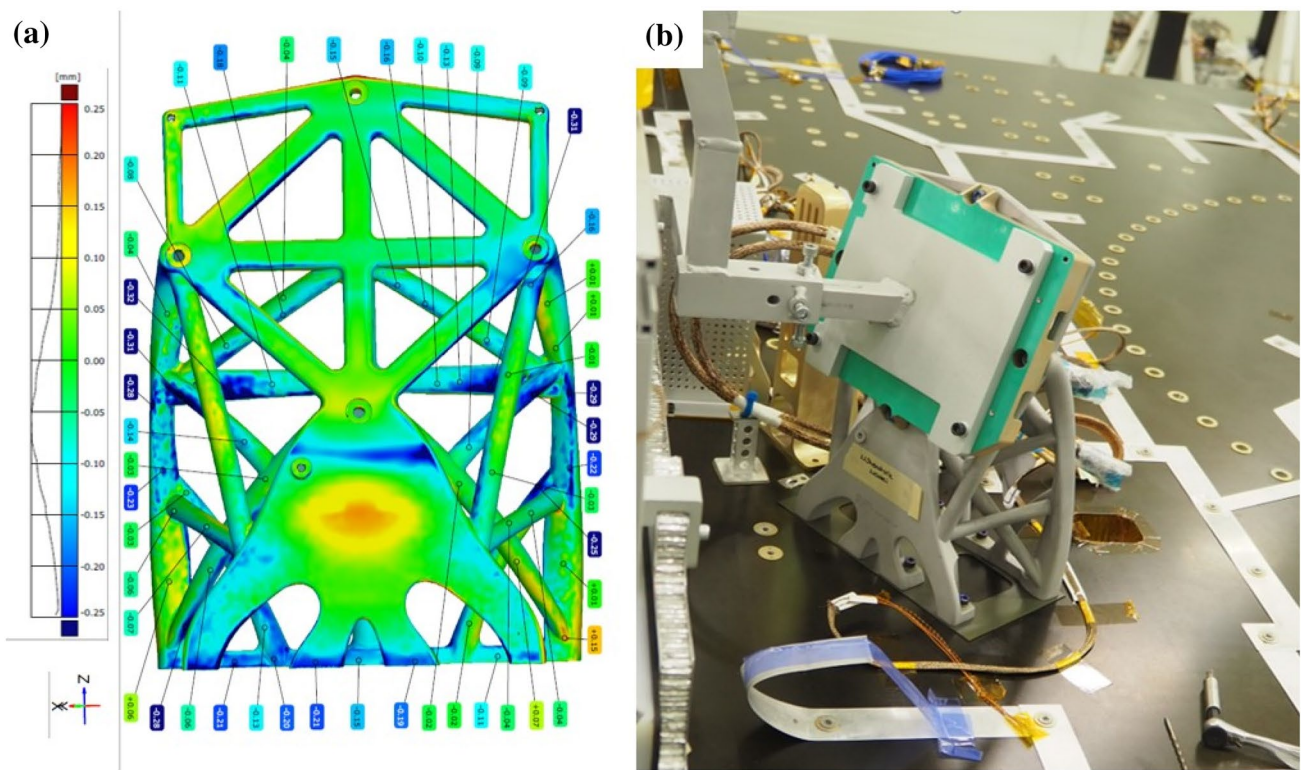**Fig. 26** Modal hammer test before-after comparison example

Fig. 27 **a** 3D scan results of the manufactured part. **b** Assembly check of STB on the satellite

coordinate measurement and 3D scan results before and after tests, there is no plastic deformation on the parts above the geometrical tolerance limits, which proved that part integrity is maintained. The 3D scan surface deviation results are given in Fig. 27a.

To check the assembly conformity after the mechanical and thermal test campaign, an assembly conformity check to the entire STB and auxiliary is held by connecting them to the satellite with the functional equipment (see Fig. 27b). In terms of connectivity and position of the star tracker, no incompatibility is observed for assembly and star tracker positioning.

4 Conclusion

In this study, an overall process from design to qualification of an additively manufactured satellite bracket is comprehensively described. The process, starting with the part selection, went forward with the performing TO. Then, the structural engineering cycle of re-design and validation practices including static, modal, sinus vibration, vibro-acoustic, shock, and thermo-elastic analyses were carried out until satisfactory results were achieved. In the experimental section, thermal testing and mechanical testing containing static, dynamic as well as shock were performed. Additionally, material-level mechanical tests and characterization techniques of AlSi10Mg were conducted according to related standards. Finally, 3D scanning and coordinate measurement were performed for the assembly control operations. From the results of this study, the following conclusions were drawn:

- TO with minimum member size and stress constraints was performed using the SIMP method. Mass saving of 25%, equivalent to 1.2 kg, was achieved comparing the original bracket designed considering the CNC manufacturing method. Thus, the launching cost including fuel cost was reduced by 15,600 $. Additionally, the environmental impact of the launching process was promised to decrease by reducing the fuel requirements.
- The minimum value of the MoS was calculated as 6 using the results of static analyses. Thus, it was shown to satisfy static requirements.
- According to modal analysis results, it was shown that the optimized bracket satisfied modal requirements by calculating first global natural frequency (152 Hz) was greater than 140 Hz which was the minimum design criterion for subsystems of the spacecraft panels.
- It was numerically proven that the optimized STB met the requirements by calculating responses of the bracket under loadings of sinus vibration, random vibration, and vibro-acoustic, and there were no exceeding values for the equipment qualification level.
- The response of the optimized STB under shock loading conditions was obtained, and it was shown that maximum stress calculated as 180 MPa was nearly 1.4 times lower than the yield strength of the AlSi10Mg material.
- According to the thermo-elastic analysis results, there is no plastic deformation calculated in the bracket assembly under the highest and lowest temperature values.

Additionally, the following conclusions were obtained from the experimental validation section:

- Dynamic tests including sinus vibration, random vibration, and shock loadings were performed to validate the optimized STB. According to test results, there was no violation of equipment qualification responses. In addition to dynamic tests, a low-level resonance search was carried out before and after the tests. Thus, it was observed that the magnitude differences of the main modes, which should be lower than 20% for tests using electro-shaker and the frequency differences of the main modes, which should be lower than 5% were within the tolerances. In the tests performed with the modal hammer, it was understood that the comparison of the modal hammer tests met the acceptance criteria of a maximum 20% amplitude difference, even if the acceptance criteria for amplitude were not defined before the tests.
- After the static tests, it was shown that there was no crack and permanent deformation, in addition to that, non-linear behavior was not observed in the load-strain curves. Therefore, the success criteria of the static test were satisfied.
- Thermal tests were performed to validate the response of the bracket under the cyclic thermal loadings. After the thermal tests, it was validated that there was no visible crack formation and the relative deflection values over the flat surfaces were within the tolerances.
- Comparative measurement control with 3D scanning and coordinate measurement showed no geometrical deviations out of the part tolerances. In addition to the dimensional measurements, assembly control of the part with satellite body and equipment was made and no incompatibility was observed.

Overall design process and qualification process of structural parts of space systems were developed with this study. As the next steps, it is planned to develop design and qualification processes for fatigue critical parts, fatigue in AM technology is a more compelling condition because of the need for post-processes to improve surface properties. On the other hand, two significant points are identified as

lessons learned from this study. The first one is that the procedure of giving overhang constraint is determined. During the iteration phase, stress constraint is observed and if it becomes a passive constraint, optimization can be stopped, and then the overhang function can be introduced as a constraint. The second one is to solve models with multiple loading conditions using weighted compliance. Finally, additively manufactured STB was qualified according to NASA and ESA standards. The STB subjected to the present study was approved to be used on a telecommunication satellite of Turkish Aerospace as further action of the project.

As a shortcoming, while RBE2 connection can converge to the experimental results in analyses, since using RBE2 adds over stiffness to the structure, it can affect material distribution at the sections where connected with RBE2 in topology optimization.

As a further study, an algorithm that performs analyses and takes required information for different load cases and topology optimization formulation including constraint functions of requirements would be developed to bypass the validation analyses and save much more engineering time. Additionally, for optimization of parts having multiple load cases, a single-objective optimization formulation minimizing the volume function considering mechanical constraints or a multi-objective optimization formulation would be developed.
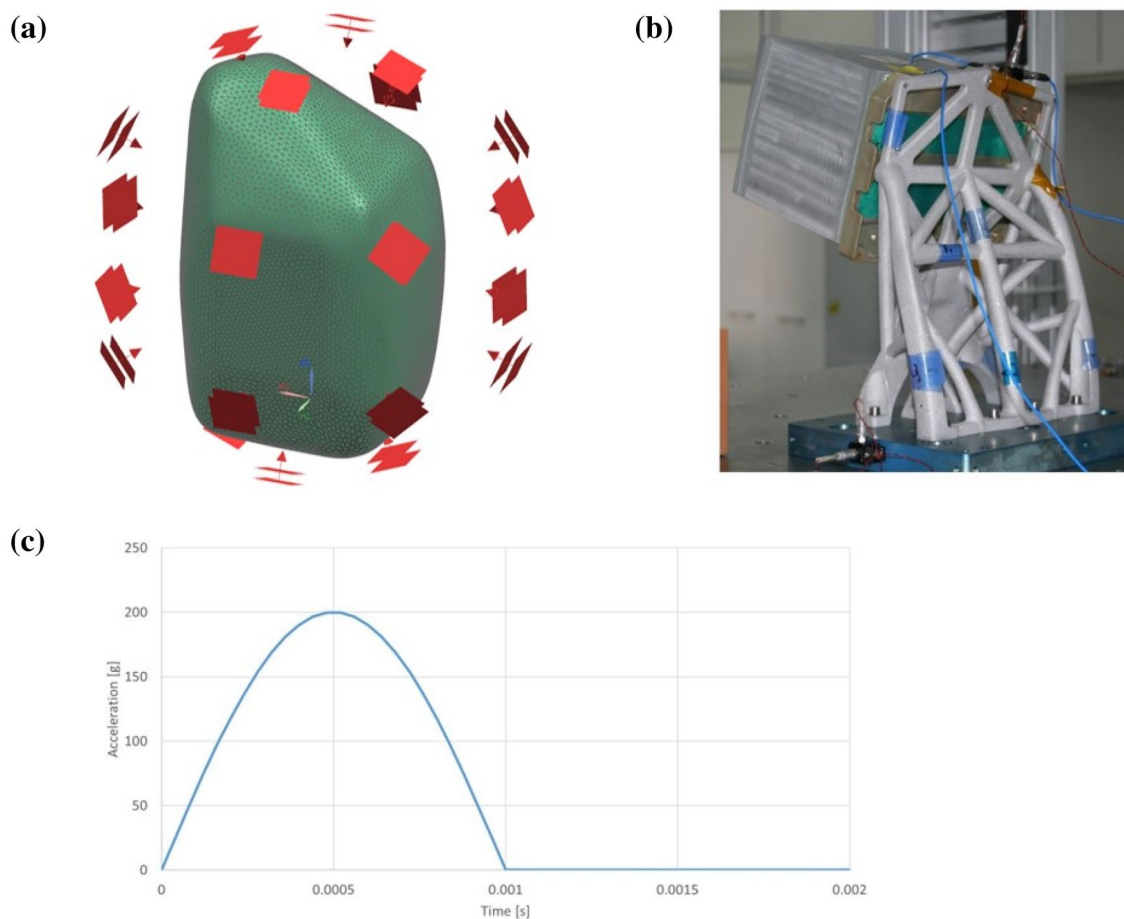
(a)

(b)

(c)

Fig. 28 **a** Acoustical plane waves visualization. **b** Shock accelerometer instrumentation. **c** Applied half-sine shock load

Appendix

Images about the vibro-acoustic analysis setup, shock test setup/instrumentation and applied shock load during time transient analyses are given in Fig. 28.

Declarations

Conflict of interest The authors declare that they have no conflict of interest.

Replication of results Loading conditions, boundary conditions and material properties of the bracket are given in Tables 1, 2 and 3, respectively. The finite element model of the bracket is confidential for the company. Additionally, the equipment qualification level is confidential and protected. The results provided herein are replicable with a similar output of topology optimization using the same inputs and the same optimization problem.

References

Allevi G, Cibeca M, Fioretti R, Marsili R, Montanini R, Rossi G (2018) Qualification of additively manufactured aerospace brackets: a comparison between thermoelastic stress analysis and theoretical results. Measurement 126:252–258. https://doi.org/10.1016/J.MEASUREMENT.2018.05.068

Altair University (2018) Practical Aspects of Structural Optimization a Study Guide. https://altairuniversity.com/freeebooks/free-ebook-practical-aspects-of-structural-optimization-a-study-guide/. Accessed 11 Jun 2022

Bendsøe MP, Kikuchi N (1988) Generating optimal topologies in structural design using a homogenization method. Comput Methods Appl Mech Eng 71:197–224. https://doi.org/10.1016/0045-7825(88)90086-2

Bombardieri R, Cavallaro R, Sanchez R, Gauger NR (2021) Aero-structural wing shape optimization assisted by algorithmic differentiation. Struct Multidisc Optim 64:739–760. https://doi.org/10.1007/s00158-021-02884-5

Braga DFO, Tavares SMO, Da Silva LFM, Moreira PM, De Castro PM (2014) Advanced design for lightweight structures: review and prospects. Prog Aerosp Sci 69:29–39. https://doi.org/10.1016/J.PAEROSCI.2014.03.003

Brujic D, Ristic M, Mattone M, Maggiore P, De Poli GP (2010) CAD based shape optimization for gas turbine component design. Struct Multidisc Optim 41:647–659. https://doi.org/10.1007/s00158-009-0442-9

Bruyneel M, Duysinx P (2005) Note on topology optimization of continuum structures including self-weight. Struct Multidisc Optim 29:245–256. https://doi.org/10.1007/s00158-004-0484-y

Chen X, Yao W, Zhao Y, Chen X, Zheng X (2018) A practical satellite layout optimization design approach based on enhanced finite-circle method. Struct Multidisc Optim 58:2635–2653. https://doi.org/10.1007/s00158-018-2042-z

ECSS Secretariat (2004) Space engineering—spacecraft mechanical loads analysis handbook. ESA Requirements and Standards Division, Noordwijk

Edke MS, Chang KH (2006) Shape optimization of heavy load carrying components for structural performance and manufacturing cost. Struct Multidisc Optim 31:344–354. https://doi.org/10.1007/s00158-005-0603-4

Gasman L (2019) Additive aerospace considered as a business. Additive manufacturing for the aerospace industry. Elsevier, Amsterdam, pp 327–340

Gradl PR, Greene SE, Protz C, Bullard B, Buzzell J, Garcia C, Wood J, Osborne R, Hulka J, Cooper KG (2018) Additive manufacturing of liquid rocket engine combustion devices: a summary of process developments and hot-fire testing results. Jt Propuls Conf 2018:1–34. https://doi.org/10.2514/6.2018-4625

Grihon S, Bassir D, Krog L (2009) Numerical optimization applied to structure sizing at AIRBUS: a multi-step process. Int J Simul Multidiscip Des Optim. https://doi.org/10.1051/ijsmdo/2009020

Ide T, Otomori M, Leiva JP, Watson BC (2014) Structural optimization methods and techniques to design light and efficient automatic transmission of vehicles with low radiated noise. Struct Multidisc Optim 50:1137–1150. https://doi.org/10.1007/s00158-014-1143-6

Koelle DE (2003) Specific transportation costs to GEO—past, present and future. Acta Astronaut 53:797–803. https://doi.org/10.1016/S0094-5765(03)80032-2

Lee DS, Fahey DW, Forster PM, Newton PJ, Wit RC, Lim LL, Owen B, Sausen R (2009) Aviation and global climate change in the 21st century. Atmos Environ 43:3520–3537. https://doi.org/10.1016/J.ATMOSENV.2009.04.024

Liu K, Tovar A (2014) An efficient 3D topology optimization code written in Matlab. Struct Multidisc Optim 50:1175–1196. https://doi.org/10.1007/s00158-014-1107-x

Munk DJ, Auld DJ, Steven GP, Vio GA (2019) On the benefits of applying topology optimization to structural design of aircraft components. Struct Multidisc Optim 60:1245–1266. https://doi.org/10.1007/s00158-019-02250-6

Nazir A, Jeng JY (2020) A high-speed additive manufacturing approach for achieving high printing speed and accuracy. Proc Inst Mech Eng C 234:2741–2749. https://doi.org/10.1177/0954406219861664

Nazir A, Abate KM, Kumar A, Jeng JY (2019) A state-of-the-art review on types, design, optimization, and additive manufacturing of cellular structures. Int J Adv Manuf Technol 104:3489–3510. https://doi.org/10.1007/s00170-019-04085-3

Orme ME, Gschweitl M, Ferrari M, Madera I, Mouriaux F (2017a) Designing for additive manufacturing: Lightweighting through topology optimization enables lunar spacecraft. J Mech Des Trans ASME 139:1–6. https://doi.org/10.1115/1.4037304

Orme ME, Gschweitl M, Ferrari M, Vernon R, Madera IJ, Yancey R, Mouriaux F (2017b) Additive manufacturing of lightweight, optimized, metallic components suitable for space flight. J Spacecr Rockets 54:1050–1059. https://doi.org/10.2514/1.A33749

Orme M, Madera I, Gschweitl M, Ferrari M (2018) Topology optimization for additive manufacturing as an enabler for light weight flight hardware. Designs 2:51. https://doi.org/10.3390/designs2040051

Remouchamps A, Bruyneel M, Fleury C, Grihon S (2011) Application of a bi-level scheme including topology optimization to the design of an aircraft pylon. Struct Multidisc Optim 44:739–750. https://doi.org/10.1007/s00158-011-0682-3

Ruess F, Segelke H, Abt F, Moratto C, Sansegundo M (2016) Acoustic analysis and testing of the Hispasat AG1 satellite proto-flight model. In: European conference on spacecraft structures, materials and environmental testing SSMET. Toulouse

Savsani VJ, Tejani GG, Patel VK, Savsani P (2017) Modified metaheuristics using random mutation for truss topology optimization with static and dynamic constraints. J Comput Des Eng 4:106–130. https://doi.org/10.1016/j.jcde.2016.10.002

Shi G, Guan C, Quan D, Wu D, Tang L, Gao T (2020) An aerospace bracket designed by thermo-elastic topology optimization and manufactured by additive manufacturing. Chin J Aeronaut 33:1252–1259. https://doi.org/10.1016/j.cja.2019.09.006

Sigmund O (2007) Morphology-based black and white filters for topology optimization. Struct Multidisc Optim 33:401–424. https://doi.org/10.1007/s00158-006-0087-x

Stolt R, Elgh F (2020) Introducing design for selective laser melting in aerospace industry. J Comput Des Eng 7:489–497. https://doi.org/10.1093/jcde/qwaa042

Talay E, Özkan C, Gürtaş E (2021) Designing lightweight diesel engine alternator support bracket with topology optimization methodology. Struct Multidisc Optim 63:2509–2529. https://doi.org/10.1007/s00158-020-02812-z

Weigel AL, Hastings DE (2004) Evaluating the cost and risk impacts of launch choices. J Spacecr Rockets 41:103–110. https://doi.org/10.2514/1.9270

Zhu JH, Hou J, Zhang WH, Li Y (2014) Structural topology optimization with constraints on multi-fastener joint loads. Struct Multidisc Optim 50:561–571. https://doi.org/10.1007/s00158-014-1071-5

Zhu JH, Li Y, Zhang WH, Hou J (2016a) Shape preserving design with structural topology optimization. Struct Multidisc Optim 53:893–906. https://doi.org/10.1007/s00158-015-1364-3

Zhu JH, Zhang WH, Xia L (2016b) Topology optimization in aircraft and aerospace structures design. Arch Comput Methods Eng 23:595–622. https://doi.org/10.1007/s11831-015-9151-2

Zhu L, Li N, Childs PRN (2018) Light-weighting in aerospace component and system design. Propuls Power Res 7:103–119. https://doi.org/10.1016/j.jppr.2018.04.001

Zhu J, Zhou H, Wang C, Zhou L, Yuan S, Zhang W (2021) A review of topology optimization for additive manufacturing: status and challenges. Chin J Aeronaut 34:91–110. https://doi.org/10.1016/j.cja.2020.09.020

Zhuang C, Xiong Z, Ding H (2021) Temperature-constrained topology optimization of nonlinear heat conduction problems. J Comput Des Eng 8:1059–1081. https://doi.org/10.1093/jcde/qwab032